Review Article

OVERVIEW OF GEOMAGNETIC DEEP SOUNDINGS (GDS) AS APPLIED IN THE PARNAÍBA BASIN, NORTH-NORTHEAST BRAZIL

B. R. Arora[1,4,5], N. B. Trivedi[1], I. Vitorello[1], A. L. Padilha[1], A. Rigoti[2] & F. H. Chamalaun[3]

Geomagnetic Deep Sounding (GDS) is an electromagnetic method of geophysics, which is capable of imaging the Earth's interior in terms of electrical conductivity using natural geomagnetic transient variations. The method is particularly suited to map geological structures marked by large lateral conductivity contrasts. An overview of the methodology is presented for a magnetometer array study undertaken within and around the intracratonic Parnaíba Basin, north-northeast Brazil. The article describes the sequential steps of data processing, the results of numerical modeling, and the related geological/tectonic implications of the inferred conductivity distribution. In the initial stages of data processing, an advanced robust regression technique is applied to derive transfer functions used to diagnose the lateral conductivity distribution in the study region. The presentation of the transfer functions in the form of induction arrows helps to identify regions of enhanced conductivity. Contour plots and pseudo-sections of the anomalous vertical fields, estimated from the hypothetical event analysis on transfer functions, are essential to characterize the orientation and dimensionality of the electrical conductive structures of the region. The analysis of various frequency and polarization parameters indicates that an anomalous behavior of the magnetovariational field, with periods longer than one hour, is determined by currents induced in the seawater, and perhaps in the raised asthenosphere beneath the oceanic region. Yet, anomalous signatures observed at periods shorter than one hour are primarily controlled by concentrated currents in two inland conductive structures. They are the Parnaíba Basin Conductivity Anomaly (PBCA), that follows the trend of the Transbrasiliano Lineament in the eastern part of the Parnaíba Basin, and the LINK anomaly, that extends from the central part of the basin to the Marajó Graben. A non-uniform thin sheet modeling has mapped the lateral extent and estimated the depth-integrated conductances of PBCA and LINK to be of the order of 2000 S and 1000 S, respectively. The overall pattern of the inferred conductivity distribution helps to visualize the LINK anomaly as relics of a probable sedimentary channel connecting the Parnaíba Basin and Marajó Graben, and which could have acted as a gateway for sea transgressions during early stages of the basin evolution. The combined inversion and forward modeling of the GDS response functions provides the PBCA structural cross-section as an ensemble of a graben-like structure in the basement and a highly conducting block confined to the deeper central part of the basin, with an embedded resistive body in the middle. The existence of a broad conducting block confined to the central part of the basin is also consistent with magnetotelluric data, and the graben-like structure in the basement is corroborated by aeromagnetic data. The origin of graben-like structures in the basement could be possibly related to an extensional tectonism, whereas the resistive body is tentatively interpreted as a diabase dike or a recrystallized magmatic body intruded during a Cretaceous magmatic event. Carbon bearing sediments are suggested as an alternative to hydrated siliciclastic sediments to account for the high conductivity of the central block. A hydrothermal event associated with the Cretaceous magmatic activity may be the likely process to produce carbon through the pyrolysis of hydrocarbon-saturated Paleozoic sediments.

Key words: Electromagnetic induction; Geomagnetic Deep Sounding; Magnetovariational fields; Electrical conductivity; Intracratonic basins; Magmatic activity.

[1] Instituto Nacional de Pesquisas Espaciais -INPE
Sao José dos Campos -SP - Brazil
[2] Departamento de Geologia, Universidade Federal do Paraná
Curitiba - Brazil
[3] School of Earth Sciences, Flinders University of South Australia,
Adelaide - Australia
[4] Permanent address : Indian Institute of Geomagnetism,Colaba, Mumbai 400005, India.

INTRODUCTION

Geomagnetic Deep Sounding (GDS) provides a view on the internal conductivity distribution, of a region of interest, from measurements of the geomagnetic transient variations at discrete geographical points. Here, we discuss the application of this technique to map the internal and deeper structure of the intracratonic Parnaíba Basin, north-northeast Brazil.

This is the first GDS experiment anywhere in Brazil (Rigoti, 1994), although the pioneering work of Schmucker (1969) across the Andes, in Peru, was critical in putting the GDS on solid footings. Over the decades, the subject has seen manifold transformation, right from the mode of data acquisition, in terms of data processing techniques, to the more significant numerical data interpretation. Further, the causes and generating mechanisms of enhanced conductivity in various tectonic environments are much better understood than before (Adam, 1997). These advances have placed the entire range of natural source electromagnetic methods as an independent geophysical tool capable of imaging the Earth's interior in terms of electrical conductivity distribution. With recent parallel advances in magnetotelluric (MT) techniques, the attention has tended to move away from the use of GDS as a method to map local structures (Banks et al., 1993). Instead, the GDS is getting a new scope as a fast and economical tool to investigate large-scale conductivity anomalies of continental scales. The EMSLAB (Electromagnetic Sounding of the Lithosphere and Beyond) experiment, and the AWAGS (Australian Wide Array of Geomagnetic Stations) are some of the outstanding examples that have given new dimensions to GDS studies. The former employed 84 magnetometers across the Juan-de Fuca Ridge (Gough et al., 1989) and the latter covered the entire Australian continent (Chamalaun & Barton, 1993). Further, when combined with even limited MT results, much more information on the structural configuration can be gleaned (Banks et al., 1996).

These aspects become quite evident in the context of the present study, which offers an illustrative case history from NNE Brazil. The focus of this article is on the overview of data processing and interpretation steps, and highlights the resolution capabilities and limitations of the technique. For reasons of brevity, only the central theme of the technique, which provides the basis for the numerical quantification, is discussed, but more details can be found in Arora (1997). For the purpose of completeness, the physical principles of the GDS are included at the very beginning. The geological and tectonic setting of the Parnaíba basin is briefly outlined to emphasize the basic rationale and layout of the magnetometer array experiment. The most immediate geological and tectonic implications of the mapped conductive structures are also summarized. The detailed account of data processing, conductive image building, functional induction modes and significance of the mapped conductivity distribution have been reported in a series of publications (Rigoti, 1994; Arora et al., 1997, 1998a, b, 1999).

PHYSICAL PRINCIPLES

In GDS, the deduction of the internal conductivity distribution is based on three time-varying geomagnetic field components, the geographic north (X), the east (Y), and the vertical (Z) components. These time-varying magnetovariational fields have their origin in the electrical current systems flowing in the ionosphere and the distant magnetosphere (Parkinson, 1983; Rao, 1997). These current systems which result from the complex interaction of solar radiation and plasma fluxes with the Earth's main magnetic field act as a natural source of electromagnetic (EM) fields. As the associated EM waves penetrate downward into the Earth, they induce currents in the electrically conducting layers of the Earth, which in turn produce their own surface magnetic fields. The depth of penetration is controlled by the skin depth d relationship expressed as follows:

$$\delta = \sqrt{(2/\mu\omega\sigma)}\,, \qquad (1)$$

where $w = 2\pi f$ is the angular frequency of the external EM field, m is the permeability and s (S/m) is the conductivity of the medium. In its simplified form, d is written as:

$$\delta = 0.5\sqrt{\rho T}\,, \qquad (2)$$

where r is the resistivity in W.m and T is the period in seconds. This relationship implies that the penetration depth increases with $\sqrt{T}$, but the actual depth of penetration depends on the unknown electrical conductivity distribution.

In theory, the relationship between external and internal magnetic fields, at a range of frequencies, holds information on the radial conductivity distribution. However, the presence of lateral electrical conductivity differences at depth perturbs the flow of induced currents and produces frequency-dependent anomalies in the X, Y and Z components. The detection of such anomalies can be facilitated by correlating data from closely spaced sites, recorded preferably by an array of simultaneously operating magnetometers. The detection and interpretation of these frequency-dependent anomalies, related to lateral electrical inhomogeneities, form the basis and objectives of the GDS technique (Schmucker,1970). In an alternative sense, the GDS combines the principle of both, soundings (depth) and profiling (lateral), to image lateral conductivity inhomogeneities at varying depths. Therefore, the method is alternatively referred to as a magnetovariational profiling (MVP)(Rokityansky, 1982), or simply as a magnetovariational (MV) study.

GEOLOGICAL AND TECTONIC SETTING

The oval shaped Parnaíba Basin is a major geological unit of the Brazilian continent, covering an area of about 600,000 km^2 in the north-northeast Brazil. Like its contemporary Amazonas and Paraná Basins (see inset in Fig. 1 for locations), the Parnaíba is composed mainly by Paleozoic sediments. All these basins are considered to represent intracratonic troughs formed over a lithosphere that underwent a major tectono-magmatic event during the late Proterozoic and early Paleozoic, i.e. during the Brasiliano orogenic cycle (Almeida et al., 1981). Thus, the Parnaíba is bounded by amalgamated fold belts that either separate the basin from surrounding cratonic regions or plunge underneath the Paleozoic sediments. In the west, the north-south trending Araguaia-Tocantins fold belt is sub-parallel to the basin and makes the transition to the Amazonas Craton. In the north, the southeastern trending Gurupi fold belt delineates the southern limits of the São Luis Craton, but plunges under the basin. In the southeast, the Rio Preto-Riacho do Pontal fold belt trends to the northeast, sub-parallel to the basin's border and to the São Francisco Craton (Cordani et al., 1884).

Also, the remarkable NE-SW trending Transbrasiliano Lineament crosses the basin from the Médio Coreaú-Curu-Independência fold belt, in the basin's northeast, to the Brasilia fold belt, in the southwest. The lineament is composed by faults and dikes that cut geological units of distinct periods, and has been related to several basement grabens found at both NE and SW ends of the basin. Cunha(1986) has shown that this important feature reflects continental tectonic events, which affected the basin throughout its evolutionary history.

In the northwest, the basin has been sectioned off from the Marajó Graben by the Paleozoic Tocantins Arch, whereas, in the north, the Cretaceous Ferrer-Urbano Santos Arch separates the Parnaíba from the São Luis and Barreirinhas continental marginal basins (Cunha, 1986). Formed during the opening of the Atlantic, these coastal basins have accumulated from 3 to 6 kilometers of Mesozoic and Cenozoic sediments, in some places over Paleozoic rocks. Structurally, the Marajó Graben is bounded by an extensive system of normal faults where older Paleozoic sediments are also believed to have been preserved (Mesner & Wooldridge, 1964; Bigarella, 1973).

The stratigraphic evolution of the Parnaíba basin is considered to have started with wide-spread Silurian sediments deposited over older Late-Proterozoic (Riachão Formation) and Cambrian-Ordovician (Mirador Formation) sediments preserved in graben-like structures in the basement (Góes & Feijó, 1994). These troughs have been interpreted as evidence of extensional tectonism at those periods (Cunha 1986; Góes et al.,1990). The basin comprises about three thousand meters of Phanerozoic sediments mostly deposited during the Paleozoic, represented by the Serra Grande (Silurian), Canindé (Devonian-Early Carboniferous), and Balsas (Late Carboniferous-Permian-Early Triassic) Groups. These rocks outcrop along the eastern and southern portion of the basin.These sedimentation cycles are separated by widespread regional discontinuities that indicate the action of slow vertical oscillations in the tectonic evolution of the Parnaíba basin (Cunha, 1986). Near the central part, the Serra Grande, Canindé and Balsas Groups account for about 2.7 km of the total thickness of 3.5 km.

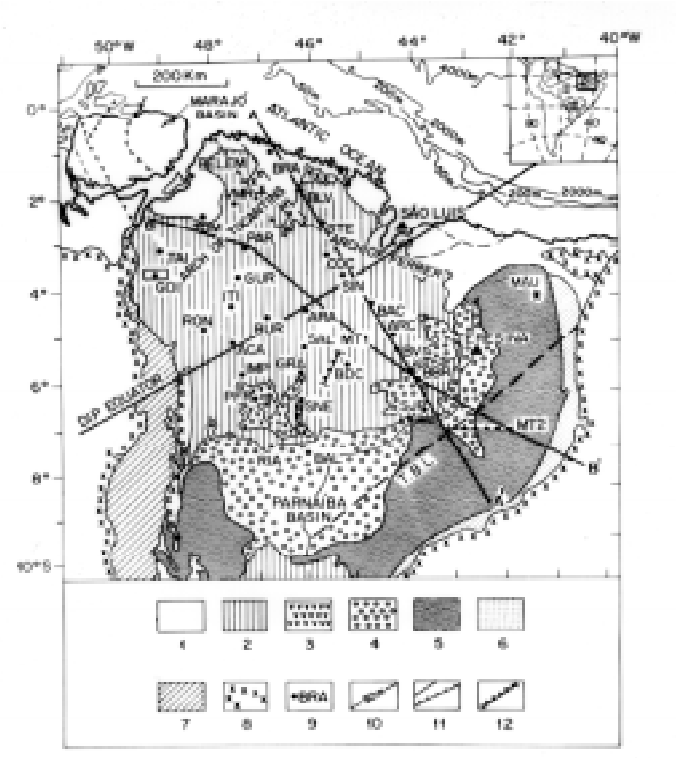

Figure 1 - Map showing the layout of the magnetometer sites (solid dots) in relation to the geology of the study area (modified from Mesner & Wooldridge, 1964, and DNPM, 1971). The geological classification was adopted from Góes & Feijó (1994), and the inset graphic legends represent:(1) Cenozoic; (2) Jurassic-Cretaceous; (3) Mesozoic volcanics; (4) Late Carboniferous-Permian-Early Triassic; (5) Devonian-Early Carboniferous; (6) Silurian, (7) Araguaia fold belt; (8) undifferentiated Precambrian; (9) magnetometer site locations and respective code names; (10) ocean depths; (11) traces of fault lines; and (12) locations of two conventional magnetotelluric profiles. The profile AA' along the eastern line of magnetometers has been used in the numerical modeling, the BB' line is the geological cross-section shown in Fig. 12a, and T.B.L. stands for the Transbrasiliano Lineament. Location of the long period MT site (MAU) is shown in the NE part of the basin. The inset shows the location of the study area and the three intracratonic basins of the Brazilian shield, namely: I - Amazonas; II – Parnaíba and III – Paraná.

Jurassic and Cretaceous sedimentary and volcanic rocks are found covering the western, central, north, and northwest portions of the basin, but rarely exceed 800 m (Góes et al., 1990, 1993; Góes & Feijó, 1994). The Mesozoic igneous activities are found in two major areas. A late Triassic-Jurassic manifestation (Mosquito Formation) predominates along N-S structures in the western part of the basin, whereas a Cretaceous volcanism (Sardinha Formation) is found mostly in NE-SW and E-W structures

located in the northeastern and eastern portions of the basin and along the Transbrasiliano Lineament (Cordani et al., 1984).

GEOLOGICAL RATIONALE FOR THE ARRAY EXPERIMENT DESIGN

While the stratigraphy and sedimentation history of the basin has been studied from outcrops and 36 scattered exploratory wells, the basement structural configuration is much less known from 21 wells that were drilled below the Serra Grande sediments (Cordani et al., 1984). Geophysical inputs have begun to appear only recently, from localized MT soundings (Oliveira & Fontes, 1991; Vitorello & Padilha, 1993 ; Lima et al., 1996), regional gravity modelling (Sousa, 1995, 1996; Sousa & Oliveira, 1995; Vidotti et al., 1995), and integrated magnetometry-gravity-seismic data (Nunes, 1993). These studies have indicated a basement of very complex structural configuration.

Thus, the application of GDS techniques is very timely. The electrical conductivity (or its reciprocal resistivity) of near-surface rocks is mainly due to the electrolyte (saline water) filling the interconnected pores. The conductivity variation resulting from the large porosity contrast between the thick sequence of sediments and non-fractured crystalline basement rocks can be useful in revealing the structural framework of the basement as well as the control of the adjoining Precambrian structures in the origin and sedimentation history of the basin.

In the absence of adequate information on the deep structural configuration, the present GDS experiment was planned to provide a regional coverage extending over a great portion of the Parnaíba Basin and contiguous area. Fig. 1 shows the layout of the magnetometer sites in relation to the major litho-tectonic units of the basin and adjoining tectonic features.

A large part of the Parnaíba Basin falls under the influence of the intense band of Equatorial Electrojet (EEJ) currents flowing in the E-region of the ionosphere, centered at the dip equator. The presence of the EEJ introduces a strong limitation in GDS applications. In the equatorial regions, this current system dominates the daytime behavior of external source currents and even modulates the induction process (Agarwal & Weaver, 1990, Chandrasekhar & Arora, 1994; Padilha et al., 1997). The adopted solution was the use of data restricted only to the nighttime interval, which eliminates data with longer periods. Consequently, the analysis of the present study tends to be confined to the upper crust. In order to comply with considerations over the souce field geometry and another major objective of the array, related to the establishment of parameters of the EEJ currents, the layout of the magnetometers was arranged along three profiles running across the dip-equator. Henceforth, these three profiles will be referred to as western, central, and eastern profiles, respectively.

DATA COLLECTION AND PROCESSING

The Flinders' digital fluxgate magnetometers (Chamalaun & Walker, 1982), with new built-in solid state memory (Chamalaun & Mcknight, 1993), were deployed simultaneously at 29 stations of the array to measure the MV fields in vertical (Z) and two horizontal components resolved to the geographic north (X) and east (Y). The measurements were carried out over a period of roughly 12 weeks, beginning in November 22, 1990. The magnetometers sampled the total field values of the three components at 1 minute intervals, with a resolution of 1 nT. The operational details and initial reduction and editing steps are outlined in Rigoti (1994).

Separation of MV Fields into Normal and Anomalous Parts

The preparation of MV data for the quantitative analysis and interpretation requires the separation of fields into parts related to its external and internal origins. Since observations are made even with a large-scale array that covers a relatively small area in comparison with the spatial wavelength of the external source fields, a separation into external and internal parts is either not possible or lacks adequate precision. This problem is circumvented by the separation of the field into its normal and anomalous parts. Such procedure is quite distinct from separating the field into its external and internal parts. In the adopted sub-division, the "normal" field is defined as a vector sum of the contributions from the external sources and that part of the internal fields which results from the induction in the stratified (one-dimensional) conductivity distribution model for the study region. The "anomalous" part is entirely due to the induction in the lateral electrically inhomogeneous media. The identification and characterization of the anomalous fields, in GDS studies, are facilitated by the following physical considerations:

(i) The induced currents in the stratified Earth portray a geometry that is simply a mirror image of the source currents. Under these conditions, the magnetic effects of external and internal currents at the Earth's surface reinforce each other in the case of horizontal components, but have a tendency to cancel each other in the vertical field component. In the limit, over a perfectly conducting half space, the X and Y are doubled while the Z is annulled.

(ii) At low and mid-latitudes, the spatial scale-lengths of the external source fields is typically several thousand kilometers and, therefore, permits the plane-wave approximation for the source fields. Under the quasi-uniform character of the source fields, the normal component of the vertical field (Zn) is negligible.

A net consequence of these two factors is that anomalous effects arising from the presence of a lateral conductivity contrast are more evident in the Z variations. This property of the Z component is much exploited in the

detection and mapping of lateral electrical inhomogeneities of the region. However, it may be noted that anomalous effects are not negligible in X and Y but, in proportion to the amplitude of the normal field, their contribution is usually small.

This classification of decomposing the observed MV fields into the normal and anomalous parts, first introduced by Schmucker (1970), is analogous to the separation of gravity and magnetic fields into regional and residual fields in the space domain. Any formulation developed in gravity and magnetic methods for this purpose can be adopted in GDS. Although sophisticated numerical techniques based on the Fourier series expansion have been developed (e.g., Wang et al., 1987), there is a more practical method of estimating the normal field. It is based on the horizontal fields recorded at a station or group of stations at a very remote distance from the anomalous zones.

Stacked Plots of Magnetograms

The assumption of spatially uniform source is fundamental to the GDS method. This assumption is invalidated in the region of the present array due to the presence of the intense band of equatorial electrojet (EEJ) currents, centered over the dip-equator during the daytime. It is known that due to the enhanced ionospheric Cowling conductivity, the source currents in all frequencies, ranging from micropulsations (Trivedi et al., 1997) to daily variations (Onwumechili, 1967), are augmented and, thus, have a non-uniform character. However, during the nighttime, in the absence of the EEJ, the MV fields are predominantly of magnetospheric origin and can be considered uniform at least for the dimension of the area.

Fig. 2 gives a typical example of nighttime MV fields, which form the basic input entities used to infer the conductivity distribution. In the example, variations were recorded on the night of November 26, 1990, when a magnetic disturbance was in progress, following the sudden commencement (SSC) at 23h and 32m UT. The magnetograms are stacked for three N-S profiles with the northern most station of each profile at the top. Both X and Y has a consistent waveform across the array, and particularly no spatial change is seen which would be a manifestation from the EEJ-like concentration of the source currents, centered over the dip-equator. This behavior suggests that the basic assumption of the plane-wave approximation is justified for the nighttime variations and the large differences in Z traces, among the stations, can reasonably be related to the local conductivity structures marked by the lateral conductivity contrast. The SSC and following short period oscillations present a reversal of sign in Z between a group of stations on the eastern profile as well as between the stations SAL and GRA. Such reversals are suggestive of conductive structures straddling between groups of stations with opposite Z variations. For the longer period Z fluctuations, station BRA is the one that presents

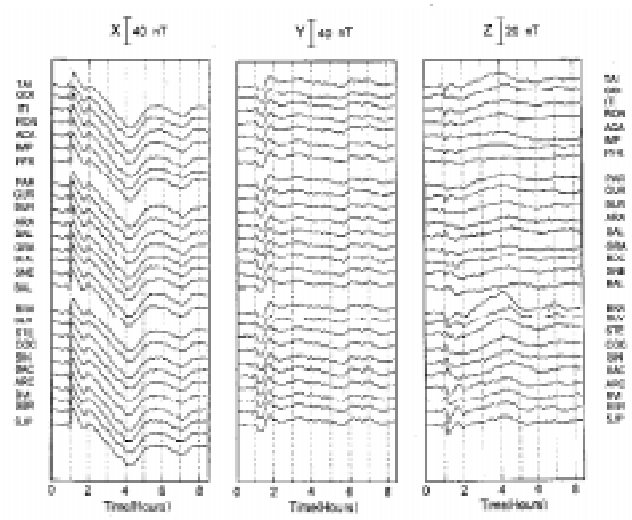

Figure 2 – Stacked plots for the three profiles of the magnetovariational fields in the north (X), east (Y), and vertical (Z) components, for 2115-0545 UT on November, 26, 1990.

the most significant differences. This behavior can be attributed to the well-known coast effect resulting from the concentration of induced currents in the seawater due to the outstanding conductivity contrast between the seawater and the land mass (Menvielle et al., 1982). In fact, the direct influence of such currents on the inland stations can be a major hazard in the detection and quantification of the inland conductivity anomalies. Therefore, the correct appraisal and quantification of the coast effect becomes an integral step of GDS data processing and numerical modeling.

A careful inspection of the stacked plots of magnetograms, or when alternatively examined in the form of Fourier transform maps, not only provides an initial diagnosis of the conductivity distribution, but is also helpful in the identification of stations or group of stations relatively free from the anomalous effects. Details of these aspects, in reference to the present array, were discussed in Arora et al. (1997), but are omitted here for brevity. However, it may be noted that the horizontal fields in the area around station GOI are located in the region of the smallest spatial gradient and, hence, could be used as a reference site to define normal field components.

Transfer Functions

The transformation of MV fields into frequency-dependent response functions suitable for quantitative interpretation is achieved through the use of a transfer function formulation presented by Schmucker (1970). A consequence of the linearity of Maxwell's EM field equations is the relationship between the anomalous and normal field components (Schmucker, 1970; Beamish,1977), which at a given frequency (period) is expressed as:

$$Z_a = T_{zx}.X_n + T_{zy}.Y_n + T_{zz}.Z_n + e_z, \qquad (3)$$

where the subscripts *'a'* and *'n'* refer to the anomalous and normal parts of the respective field components. The

assumption of a quasi-uniform external source field permits to neglect Z_n, as it tends to be negligibly small. Also, in a linear system, the components of the normal horizontal field (X_n and Y_n) are the input, and the anomalous vertical field (Z_a) is the output determined by the response characteristics (set of T's) of a filter represented by the unknown conductivity structure. A reference site could be chosen whose fields could be taken as a measure of normal fields. The transfer functions so defined are referred to as the inter-station (common reference) transfer functions. When only data from single sites, operated one at a time, are available, the functional assumption is that anomalous parts of the horizontal fields are small and, hence, the observed horizontal fields at individual sites can be substituted for the X_n and Y_n. Transfer functions calculated in this manner are termed single-station transfer function. According to F. E. M. (Ted) Lilley (personal communication), sometimes the anomalous parts are not small and may reach 10% or even more than 20%. In such cases there is a significant error introduced when the transfer function estimates are subsequently used in the hypothetical event tecnique. The present work avoids this difficulty because it has simultaneous array data and takes station GOI as reference station for the horizontal field variations.

The spectral formulation by which array data may be processed to obtain transfer functions has been described in detail in Schmucker (1970) and Everett & Hyndmann (1967). Most of the variant methods adopted to estimate transfer functions have relied on the least square solutions (LS), in the sense that a best fit to the above expression (Eq.(3)) can be found so that the error term (e) is minimized. In the present study, the evaluation of the statistically reliable transfer functions was carried out using the state-of-art technique of robust regression (Egbert & Booker, 1986). The technique does not make any assumption on the Gaussian error distribution, implicit in LS methods, as well as down weights the influence of high power events, which tend to dominate in the LS approach.

In the adoption of this method to the present dataset, data of some 52 nighttime segments were used. The choice of the segments was based on their wide frequency content and varied polarization. In the computations of inter-station transfer functions, the horizontal fields recorded at the station GOI were reckoned to be the measure of normal field. The complete computational details are given in Arora et al. (1997, 1998a). Basically, a three level decimation by a factor of four was successively used so that a fixed 128-point FFT window, with a 25% overlap, enabled an estimation of transfer functions for 13 bands in the period range of 6 to 132 minutes. This choice of the range of frequencies (period) analyzed was limited by the following factors: the sampling interval of 1 minute and the sensitivity of 1 nT of the magnetometers, determined the resolution of the shortest period (~6 min). The limiting factor on the longer period was the source field geometry that restricted the data to nigthtime segments. To minimize the effects of non-uniform sources, only variations not influenced by the daily variation fields have been processed.

Induction Arrow Presentation

To display and isolate the information contained in the transfer functions on the conductivity distribution in the vicinity of the measuring sites, maps of induction arrows are, by far, the best manner to make the presentation. The complex transfer functions are used to define a pair of induction arrows, each corresponding to the real and quadrature parts. The magnitude of the real and quadrature induction arrows is given by:

$$S_r = \sqrt{(Re(T_{zx}))^2 + (Re(T_{zy}))^2}$$
$$S_i = \sqrt{(Im(T_{zx}))^2 + (Im(T_{zy}))^2}\ , \qquad (4)$$

whereas the corresponding azimuths are obtained as follows:

$$\theta_r = tan^{-1}\ (Re(T_{zy})/Re(T_{zx})),$$
$$\theta_i = tan^{-1}\ (Im(T_{zy})/Im(T_{zx}))\,. \qquad (5)$$

It is a usual practice to reverse the azimuths so that, in their graphical presentation with respect to the geographic north, arrows point at right angle to the current concentrations and, hence, define the strike directions of the conductive structures causing concentrations of the induced currents (Gregori & Lanzerotti, 1980). Their lengths (magnitudes), being a measure of the anomalous vertical field normalized to the strength of the inducing field, are the requisite GDS (MV) response function characterizing the electrical and geometrical parameters of the involved structures.

CONDUCTIVE IMAGE BUILDING

Fig. 3 gives the maps of the real and quadrature induction arrows for three periods. The arrow maps at the short periods of 12 minutes bring out evidence on the presence of many conductive zones within the study region. The salient induction features of the involved conductive structures are summarized below:

a) The Parnaíba Basin Conductivity Anomaly (PBCA)

On the extreme south of the eastern profile, the real induction arrows, shown in the upper left diagram of Fig. 3, at stations SJP and BBR, point to the NNW, clearly indicating a current concentration to the north along an ENE-WSW path. Further up on the eastern profile, the arrows at the STE, COC and SIN stations are directed SSE, limiting the position of the current concentration to within SIN (or BAC) and BBR, where arrows directed in the opposite directions attain the maximum magnitude. This anomalous pattern in the southeastern part of the array is referred to as the Parnaíba

Basin Conductivity Anomaly (PBCA). The northeast pointing arrows at SNE and GRA define the southwestern terminal edge of the PBCA on the southwest. The near-vanishing real arrow at BDC, with Z tending to zero, suggests the proximity of the station to the axis of the PBCA. The station BDC is located close to the center of the basin where the thickness of the sedimentary column is largest, permitting an inference that induced currents must be flowing in the sedimentary columns. A rather unusual but persistent feature of the arrow pattern associated with the PBCA is that, near the central part of this anomaly, the induction arrows at ARC and BVI point away rather than towards the central axis. This arrow pattern is considered to mark the presence of a localized heterogeneity, such as a resistive body embedded within the PBCA. The reversal in the direction of the induction arrows between GRA and SAL may be seen as a narrow linear elongation of the PBCA between this pair of stations.

b) The LINK anomaly

In the extreme northwestern corner of the array, the S-SW pointing arrow at TOM, as opposed to the N-NE directed arrows at TAI, suggests the presence of another elongated structure between the stations TOM and TAI. The structure Marajó Graben towards the PBCA anomaly, at the central part of the Parnaíba Basin, as evidenced by the near zero magnitude arrow at PAR. This anomalous pattern extending from the region of the Marajó Graben towards the Parnaíba Basin has been named the LINK anomaly. Perhaps, under the influence of the current concentration in this structure, the induction arrows at all stations point uniformly in the N-NE direction.

c) The influence of the Atlantic Ocean

The near-north pointing arrow at BRA represents the conventional geomagnetic coast effect related to the concentration of induced currents in the conducting sea-water. This influence of such oceanic currents is found to increase at increasingly longer periods (upper panels in Fig. 3). For example, the real induction arrows at stations BLV, STE, and COC, in the northwestern part of the array, swing from their directions at 12 minutes to a perpendicular position to the nearest coastline, at 43 minutes. The geographical area over which this rotational behavior is noticed gradually expands land-wards, until the real arrows at all array stations tend to point uniformly in the northeastern direction, towards the deep Atlantic ocean, at a period of 79 minutes, or higher (Menvielle et al.,1982). The dominance of this behavior at

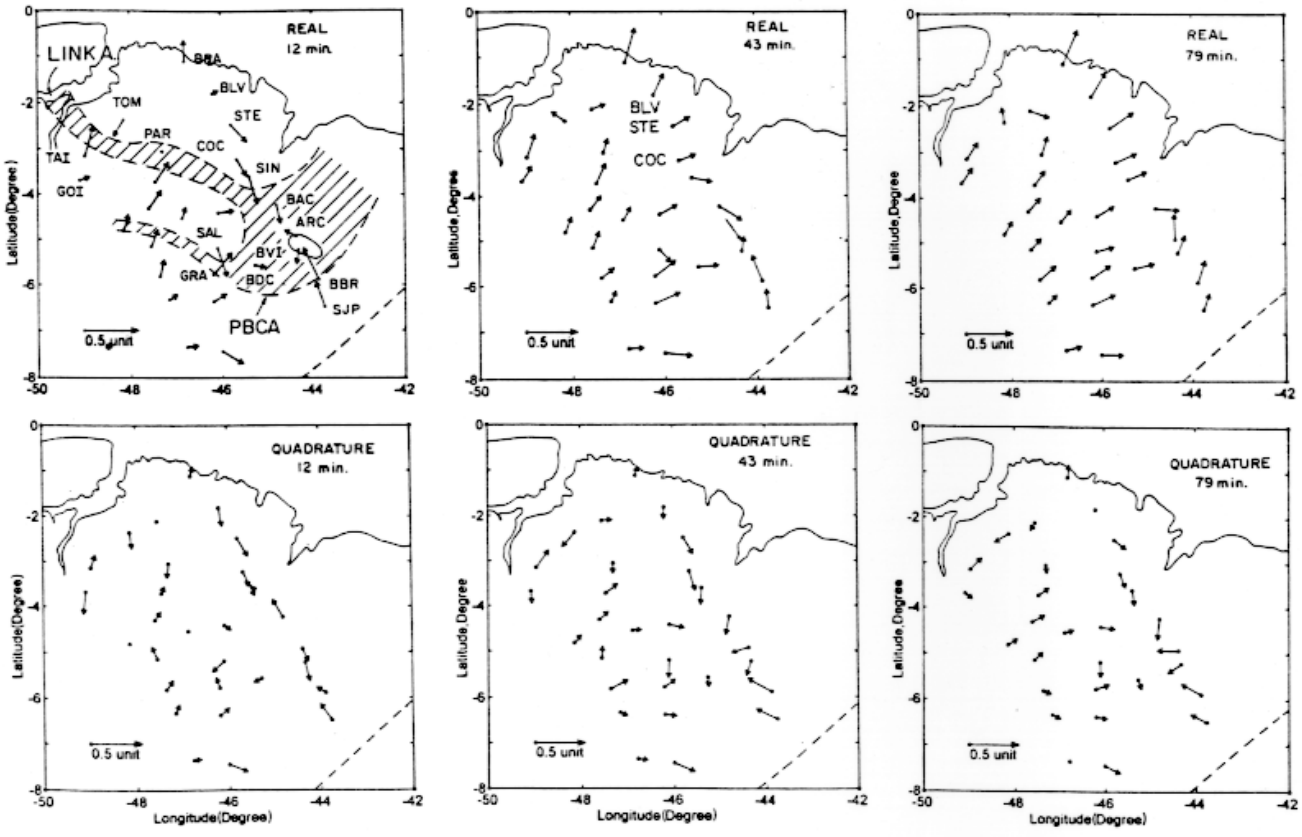

induction arrow pattern at the 12 minutes period marks the location of two high conductivity zones (PBCA and LINK anomalies). Only the code names of stations that help to define the two anomalies are shown.

induction in the raised asthenosphere beneath the oceanic region is also an important component.

d) The Southern Structure

The presence of a detached structure, south of the main anomalies and approximately aligned with the trend of the Transbrasiliano Lineament, is indicated by the southeastern pointing induction arrows at BAL. However, the absence of other stations SE of the study region prevents the determination of the position and the extent of the current concentration associated with this conductive feature.

ELECTRICAL CHARACTERISTICS OF THE STRUCTURES

The accompanying quadrature arrows (lower panel in Fig. 3) at short periods, for example at 12 minutes, portray a spatial pattern that corroborates the interpretation offered by the maps of real induction arrows. However, the quadrature arrows do not exhibit the rotational dependence at longer periods, shown by the real arrows. Instead, even at long periods, they continue to define the inland conductive structures, identified by the short period arrows. This distinct period-dependent behavior of the real and quadrature arrows derives from their varied sensitivity to the electrical type, either reactive or resistive, of the conductors carrying the induced currents (Gough et al., 1974). In structures whose electrical properties are dominated by inductance rather than resistance, the induced currents would be largely in-phase with the inducing fields. In such cases, only the real induction arrows would prevail. However, in sedimentary basins, where the resistance exceeds the inductance, a considerable phase difference would occur between induced and inducing fields, leading to substantial quadrature arrows that accompany the real arrows. In the light of this expected behavior, it can be surmised that at short periods both real and quadrature arrows are controlled by currents in sedimentary columns of the basin. But as the periods increase, the real arrow behavior is predominantly determined by currents in the oceanic regions, where the induced fields are in-phase with the inducing fields (Gough & Ingham, 1983). Nevertheless, quadrature arrows still point to the near inland sedimentary structures due to their sensitivity to the out-of-phase currents.

HYPOTHETICAL EVENT ANALYSIS

Returning to the linear system analogy, knowing the transfer functions in Eq. (3), the output can be determined for a given input. Say, for example, that the real (Z_r) and the imaginary (Z_i) parts of the anomalous vertical fields, that would be produced by the horizontal field of unit amplitude, at an azimuth (polarization) of θ° with respect to north, are given by:

$$Z_r = Re(T_{zx})\cos\theta + Re(T_{zy})\sin\theta, \qquad (6)$$

$$Z_i = Im(T_{zx})\cos\theta + Im(T_{zy})\sin\theta. \qquad (7)$$

This technique was termed Hypothetical Event Analysis (HEA) by Bailey et al. (1974). The predicted values of Z_r (or Z_i) at a given period and polarization can be utilized to produce maps of the anomalous fields. The advantage of the HEA approach is that multiple stations transfer functions obtained from non-simultaneous sub-arrays, run either with a common reference site or only one at a time, can be combined to generate large synthetic array maps (Beamish & Banks, 1983). In case only single station transfer functions are available, sophisticated techniques have been developed to estimate anomalous vertical fields free from the bias due to the presence of anomalous horizontal fields at individual sites (Banks, 1986; Parkinson, 1989)

The interest to simulate such maps stems from the fact that the study of the changing response of the conductive structures to a varying azimuth of the incident horizontal field can be a useful guide to infer the strike and the geometrical dimensionality of the involved structures.

In an ideal 2-D case, the strongest response would be seen when the horizontal field is polarized at right angles to the strike, while the response would vanish for the orthogonal direction. Fig. 4 gives the contour plot of Z_r for the region of the present study, at the period of 12 minutes, when the azimuth changed progressively from N60°W to N90°E, in steps of 30°. The presence of the PBCA and LINK anomalies are seen as pairs of twin-vortex of positive and negative values, in the southeast and northwest parts of the array, respectively. The immediate feature to catch attention is that the vortex pattern waxes and wanes with the changing polarization of the horizontal field. The response of the PBCA is best developed in association with the horizontal field polarized N30°W, whereas the pattern almost diffuses for the orthogonal polarization. Similarly, the maximum response of the LINK anomaly is seen with a polarization of N30°E and a corresponding minimum is found for a polarization of N60°W.

These observed response characteristics suggest that the induction responses of the PBCA and LINK anomalies are compatible with the elongated structures oriented respectively N60°E and N60°W. Large gradients in the region of stations SAL and GRA are indicative of a large current density and are, therefore, to be associated with an exceptionally high conductivity contrast and/or with an intense geometrical concentration of currents.

A PSEUDO-SECTION OF ANOMALOUS VERTICAL FIELDS

A qualitative idea on the depth extent of each individual conductive structure can be obtained from a pseudo-section of the real and/or quadrature parts of the anomalous vertical field (Z_r/Z_i). The sections can be obtained for the polarizations of the incident source field that maximizes the induction in the involved structure (Gough & Ingham, 1983). For example, in Fig. 5a, the Z_r values, corresponding to the

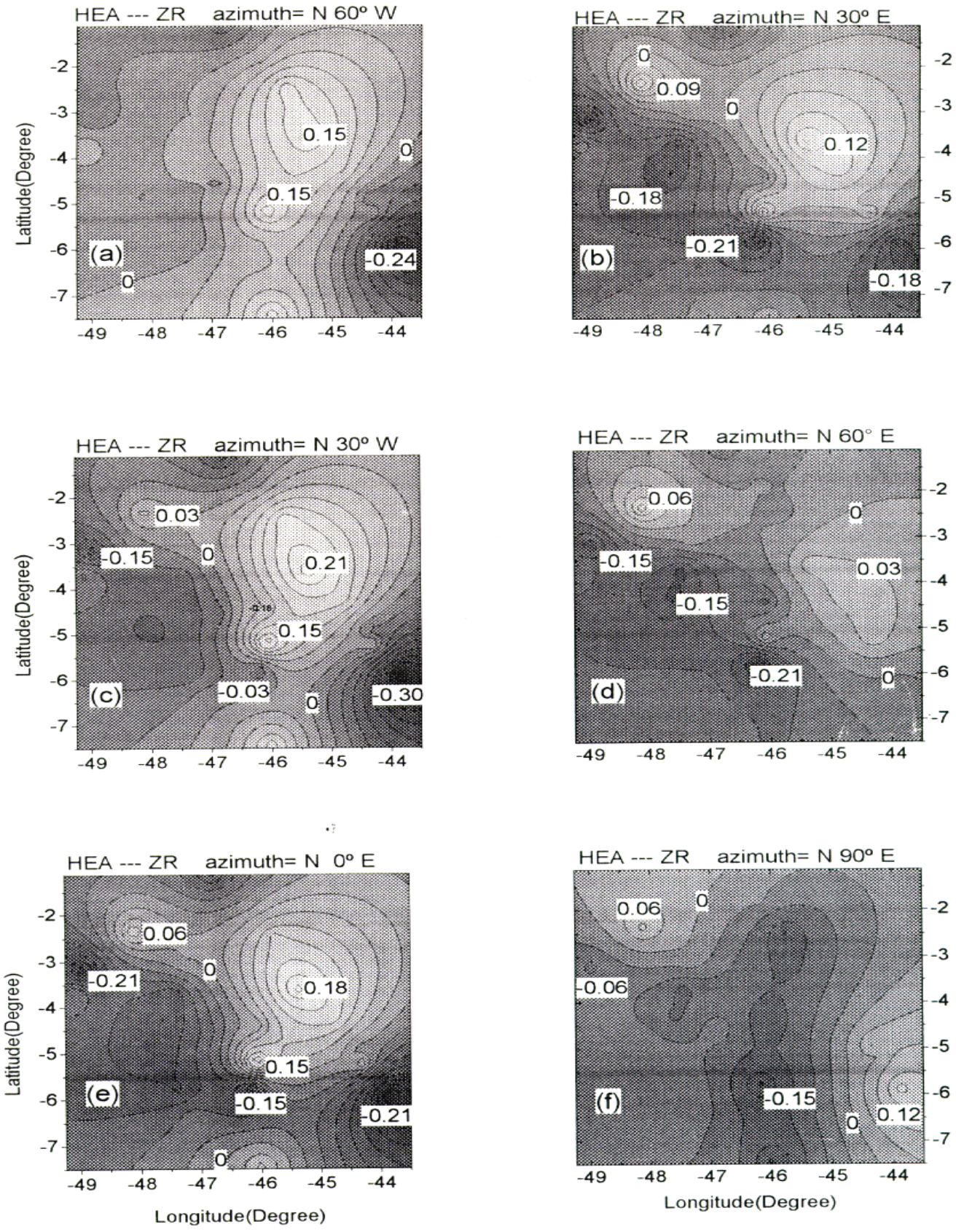

Figure 4 - Smoothed contour maps of the HEA predicted real part of the anomalous vertical field (Z_r) at the 12 minutes period, for the range of horizontal field polarization.

polarization of N30°W, are estimated by performing the HEA on all the 13 bands of the transfer functions, for a group of stations on the eastern profile. In the pseudo-section, the horizontal scale is the distance of the sites along the profile and the vertical scale is the square root of the period (T), a function of the penetration depth (Eq. 2). Consistent with the sign convention for the induction arrows, the sign of Z_r has also been reversed on the pseudo-section, and, thus, a negative zone indicates a conductive source to the right, and a positive zone indicates a source to the left. At periods shorter than an hour, a well-defined couplet of positive and negative contours in Fig. 5a indicates a high conductivity zone embedded between the locations of extreme Z_r values at stations SIN and BBR.

Although the pseudo-section does not provide information on the true depths of the conductive zones, the dominance of the measured response at relatively low periods can be construed to infer relatively shallow depths of the involved structures. Similarly, the observation that a pronounced negative zone, extending over stations COC to BVI, wanes at higher periods implies that the structure associated with the PBCA narrows down in width, but extends to greater depths only beneath the BAC-ARC stations. The profiles of Z_r at some selected periods, shown later in Fig.13, are also useful modes of displaying the observed induction response for comparison with the numerical response of the geo-electrical models to be developed. Such profiles also clearly show the small-scale features that are not well enhanced on the pseudo-sections in Fig. 5, due to the dominance of the regional anomalies.

Polarization at N60°E, corresponding to the pseudo-section in Fig.5b, is not a favorable direction to show the response from the PBCA, but is appropriate for the indication of electric currents in the oceanic region. The high values of the Z_r seen beneath the BRA station and its decaying trend away from the coast line can be attributed to the coast effect (Menvielle et al., 1982). The fields of these oceanic currents are superimposed and tend to dominate the magnetic fields associated with the inland structures at periods greater than an hour. As a consequence, at these long periods, the induction arrows at all stations (Fig. 3) point NE towards the current flowing in the deep Atlantic ocean (Arora et al., 1997).

RELATION TO MAGNETOTELLURIC SOUNDINGS

The anomalous electric character of the Parnaíba Basin was also indicated by conventional magnetotelluric (MT) soundings made by Oliveira & Fontes (1991). These authors made MT measurements in the frequency band of 500 Hz to 0.01 Hz, on two short profiles in the central and southeastern portions of the basin, marked in Fig.1 as MT1 and MT2, respectively. Fig.6a gives the typical apparent resistivity and phase sounding curve of the profile MT1. The 1-D inversion of the sounding curves presents a 3-layer

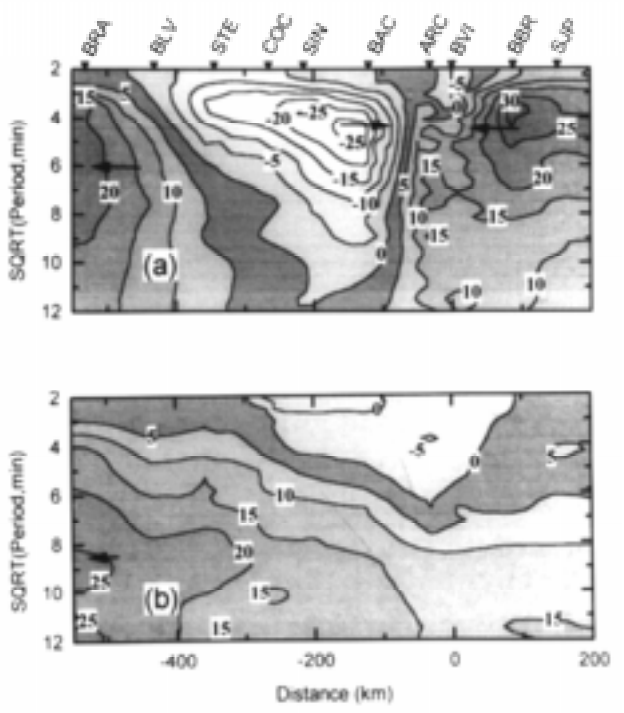

Figure 5 – The eastern pseudo-section of the real part of the anomalous vertical field (Z_r x100) associated with unit amplitude horizontal field polarized in N30°W, shown in (a), and in N60°E, shown in (b). Arrows point towards regions of higher conductivity.

structure for the sedimentary column above the basement (Fig.6b). The upper two layers, with resistivities of 50 Ω.m. and 10 Ω.m, present appropriate values for the exposed Jurassic-Cretaceous formations and underlying Balsas Group, respectively. The third layer, with a resistive value well below 1 Ω.m is the most dominant feature of the sedimentary section above the basement. The other profile, MT2, near the fringe of the basin, indicates the presence of a relatively less conducting layer, of about 10 Ω.m, above the sediment-basement interface (Lima et al., 1996). This observation suggests that the highly PBCA conductive zone is primarily confined to the central part of the basin.

This evidence of a highly conducting structure confined to the central part of the Parnaíba Basin, both by MV and MT techniques, known respectively for better lateral and vertical conductivity resolution, has important cognitive consequences (Banks et al., 1996). First, the MV response measured in a 2-D spatial domain is a valuable manner of determining the lateral extent and overall conductance by the recourse to the thin-sheet modeling. Second, the high resolution resistivity-depth distribution provided by the localized MT surveys can be used as a guide to interpret numerically the MV response in order to constrain the vertical configuration of the structure associated with the PBCA. Theses considerations form the basis for the numerical interpretation of the GDS response function, discussed in the following section.

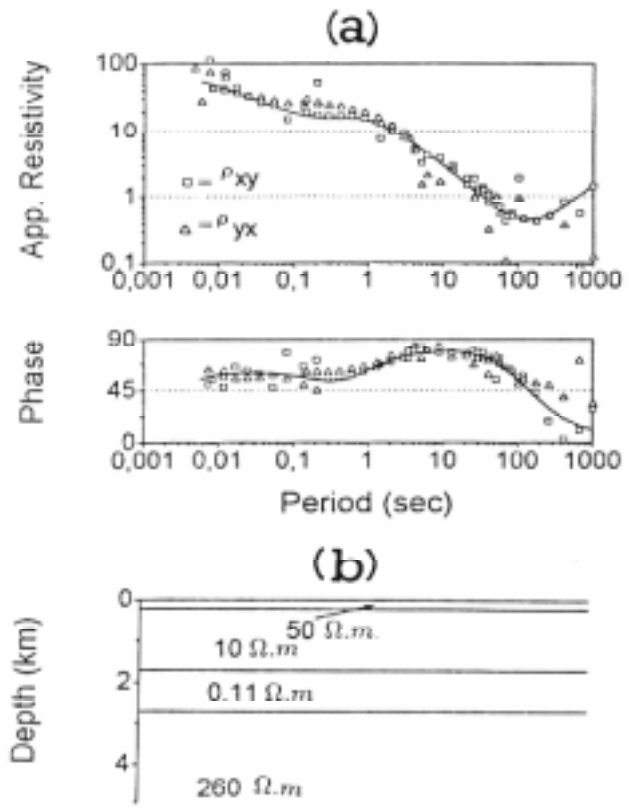

and phases are shown for measured (dotted lines) and interpreted (continuous lines) data; in (b) it is shown the inverted 1-D electrical section of the MT sounding.

NUMERICAL MODELING

The information on the geometry and electrical parameters of the involved structures can be gleaned by seeking forward- and inverse- solutions of the GDS response functions established both in spatial and frequency domains. In GDS, modeling exercises have mostly relied on 2-D and 3-D forward schemes. The 2-D forward modeling is now routinely used but they lack uniqueness. The major uncertainties result from the following inherent limitations:

(i) Because a separation of fields into internal and external parts is not possible, the change of conductivity with depth in the survey area remain unknown. The numerical modeling of anomalous fields has to be approximated by lateral conductivity changes within a preconceived layered conductivity distribution. To place realistic constraints, radial conductivity distribution must be inferred from independent sources.

(ii) Even at the shortest period commonly used in GDS (~5 minutes in the present study), the penetration depth exceeds several tens of kilometers. Hence, frequencies (periods) that yield a distinct response of the top and bottom of a very shallow structure are not available. Further, the measured response at longer periods is dependent on the conductivity distribution to the full skin-depth, which goes down to several hundred kilometers. Therefore, the parameters of shallow structures have to be inferred from the range of frequencies where the effects of shallow structures are greatly blurred.

A net consequence of the above factors is that the GDS depth resolution is poor. A good depth constraint can be provided by available magnetotelluric data. Furthermore, the validity of the proposed geo-electrical model should be tested in the light of the geological background of the area and available geophysical information.

Inversions of the GDS response functions to a conductivity model suffer from the fact that they are not a well-posed inversion problem (Sriniwas, 1997). Banks (1979, 1986) has shown that the 2-D inversion of a MV response to an equivalent current distribution is a more tractable problem than the direct deduction of conductive distribution models. The technique, which locates such current concentrations, effectively defines the structural boundaries of the region of enhanced conductivity. This property can be a useful guide in defining the structural configuration at least for the purpose of approximating the initial conductivity distribution models to be tested by a comprehensive 2-D forward modeling. The combined approach of 2-D current inversion and 2-D conductivity forward modeling is applied below to model the GDS response of the PBCA on the eastern profile, where the induction response is found to be compatible with the induction in a 2-D structure.

Applications of full 3-D algorithms, although available, are less popular due to their requirements on large computer time and memory storage, even when only a simple 3-D geometry is modeled. Instead, an alternative approach to simulate a 3-D structure, or where the presence of multiple interactive conductors is indicated, is the use of a 3-D thin sheet formulation to quantitatively constrain the depth-integrated conductance of the mapped structures. In view of the known success of this approach to model electromagnetic effects in sedimentary basins (Menvielle et al., 1982; Agarwal & Weaver, 1990), the thin sheet formulation has been used successfully to develop the regional conductance map of the north-northeast Brazil with estimations of the extension and conductance values of various conductive structures inferred by the present array of magnetometers.

Thin Sheet Modeling

The thin sheet formulation considers that the conductivity anomalies are confined to a single layer at the surface of the Earth. In such cases, the mathematical model used comprises an infinitesimally thin sheet of varying surface conductance underlain by a layered half space (Fig. 7). In modeling regional data, it is usual to assign an equivalent thickness, such that the conductance may be thought of as the conductivity integrated vertically through the thickness of the sheet. The limit on the thickness of the sheet is provided by the conductivity of the material

constituting the sheet as well as by the linked eletrical substratum so that, at the periods of investigation, the horizontal electrical field remains constant over the thickness of the sheet (Weaver, 1982). This statement implies the condition that the thickness of the sheet should be small compared with the skin-depth of the diffusing EM wave, in the layer immediately beneath the sheet, at the considered period. A second condition is that the sheet thickness should be very small in relation to the skin-depth in any material included in the sheet.

In agreement with these conditions, a thin sheet was assigned a thickness of 6 km that allowed a reasonable incorporation of the thick strata of inland sediments as well as an ocean with different depths. The thin sheet was considered to be overlying a four-layer conductive Earth model, shown in Fig. 7. The choice of the background layered-structure was based on the geo-electrical model determined by the long period MT sounding made at the station MAU (Fig.1), some 200 km east of the station BAC (Stoerzel, 1996).

At present, there are two well-known algorithms for numerical solutions of induction in non-uniform thin sheet, developed by Vasseur & Weidelt (1977) and Mckirdy et al. (1985), respectively. The algorithm of Vasseur & Weidelt (1977) requires that the anomalous domain in the sheet should be surrounded entirely by a uniform region. The algorithm of Mckirdy et al.(1985) requires that the outward gradient of the conductance should vanish at infinity.

In the present study, the algorithm of Vasseur & Weidelt (1977) is adopted because it needs less computational time and memory storage. The total area shown in Fig.1 was considered in the analysis, in order to minimize the effect of artificially confining the anomalous observational domain by a uniform structure. The total area is much larger than the actual observational domain. A large continental shelf and oceanic region is included to reproduce the oceanic effect.

For the purpose of numerical computation, an area of roughly 11^{o} x 11^{o} was divided into 44x44 grid with a node spacing of 27.5 km. The geological features guided the boundaries of the variable conductance whereas the assignment of conductance values to the cells relied on the information from the magnetotelluric surveys in the central part of the Parnaíba Basin (Oliveira & Fontes, 1991) as well as in the adjacent Paraná Basin (Stanley et al., 1985). For the purpose of assigning initial conductance, estimates on the thickness of individual geological units and total sedimentary columns in the Parnaíba Basin and Marajó Graben were based on the contour maps of isopachs and geological cross-sections (DNPM, 1971; Caputo & Lima, 1984; Góes et al., 1990). The conductance values of the cells over the oceanic region was proportional to the mean depth of seawater between successive bathymetric contour lines. The complete procedure and basis for the initial conductance distribution are described in Arora et al., 1998a). The different categories of conductances as well as geometrical parameters (thickness and grid size) of the thin

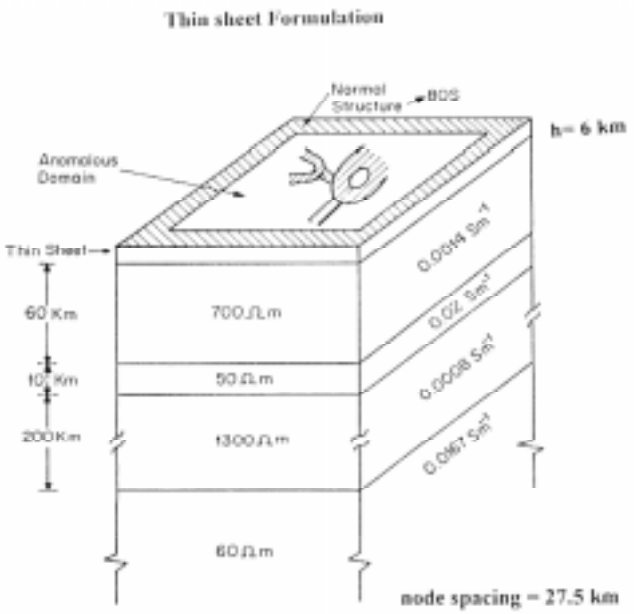

Figure 7 – Illustration shows the adopted model of the thin sheet configuration and of underlying layered structures, for north-northeast Brazil. The thin sheet with an equivalent thickness of 6 km is represented by 44x44 grid, with a grid spacing of 27.5 km.

sheet satisfied the conditions necessary to validate the thin sheet approximation (Weaver, 1982).

The initial model which considered the conductance distribution symmetric with respect to the deepest part of the Parnaíba basin and closely followed the isopach contours could not explain the most salient features of the observed induction pattern. Recognizing that the existing information on the regional variation of the thickness of sediments provides only a crude approximation, conductance values of certain cells, particularly in the central part of the Parnaíba and Marajó Basins and their lateral configurations, were changed in a trial and error procedure. Fig. 8 shows, in coded form, the distribution of depth-integrated conductance values, whose induction responses reproduced the observed induction pattern quite satisfactorily. The comparison of the model and observed induction arrows, both in its real and quadrature parts, is shown in Fig.9. The modeled real and quadrature arrows provide a reasonable good fit to the observed pattern, which enhances the confidence in the deduced conductivity distribution pattern. The overall picture of the conductance distribution in the study region is shown in Fig. 10.

In the attempt to reproduce both directional and spatial magnitude patterns, the thin sheet model approximates the PBCA as a roughly 200 km wide NE-SW elongated structure with a conductance of 2000 S in the central part. The southwestern terminal edge is seen as an arc with a minor NW elongation on the western flank, which is able to account for the sharp reversal of the induction arrows between stations GRA and SAL. A low conductance (resistive) strip within the PBCA reproduces the reversal of arrows at ARC and BVI and suggests a local heterogeneity near the central

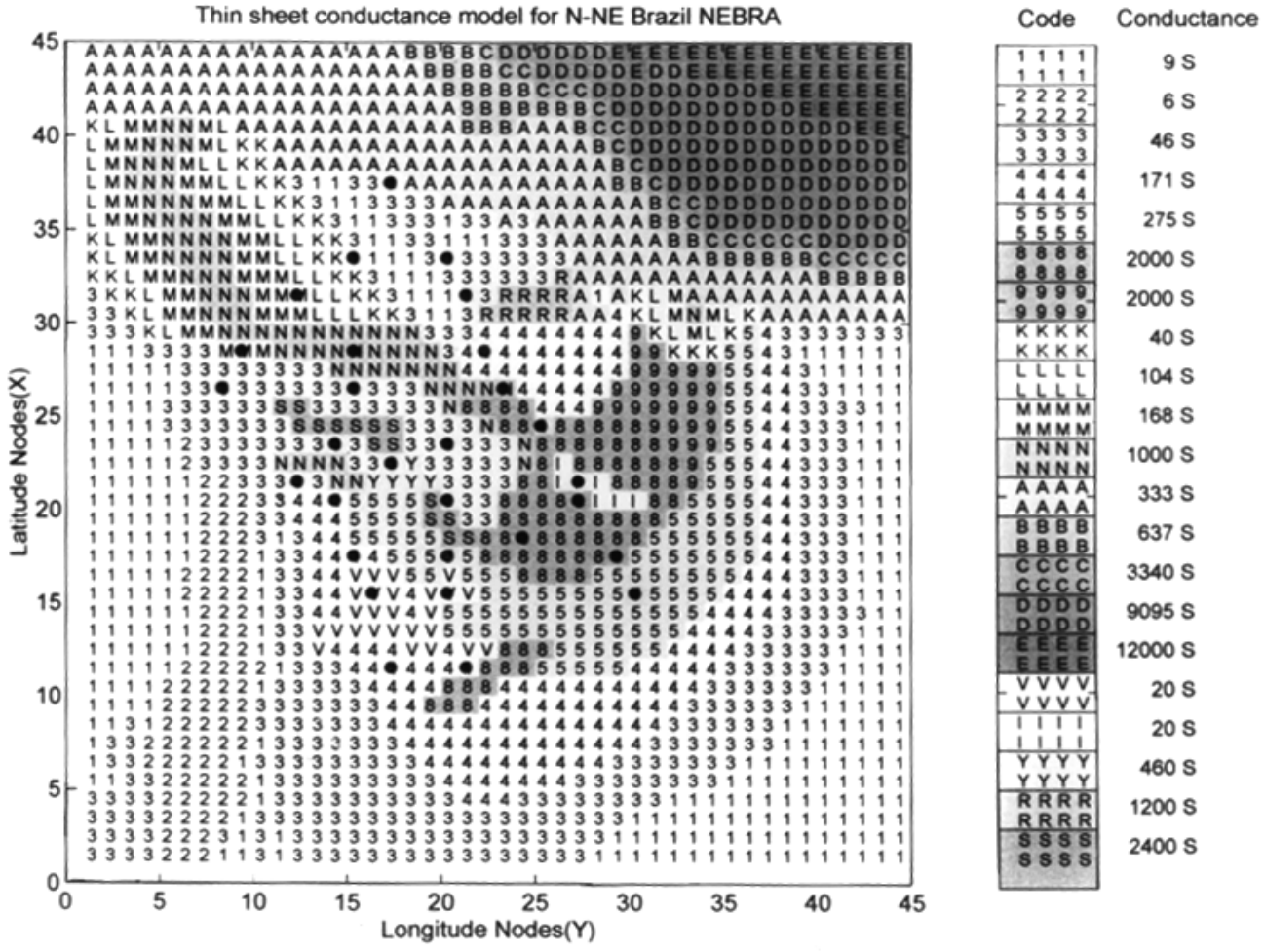

Figure 8 - Conductance codes depicting distribution of conductance values in the thin sheet model for north-northeast Brazil. Nodes denote

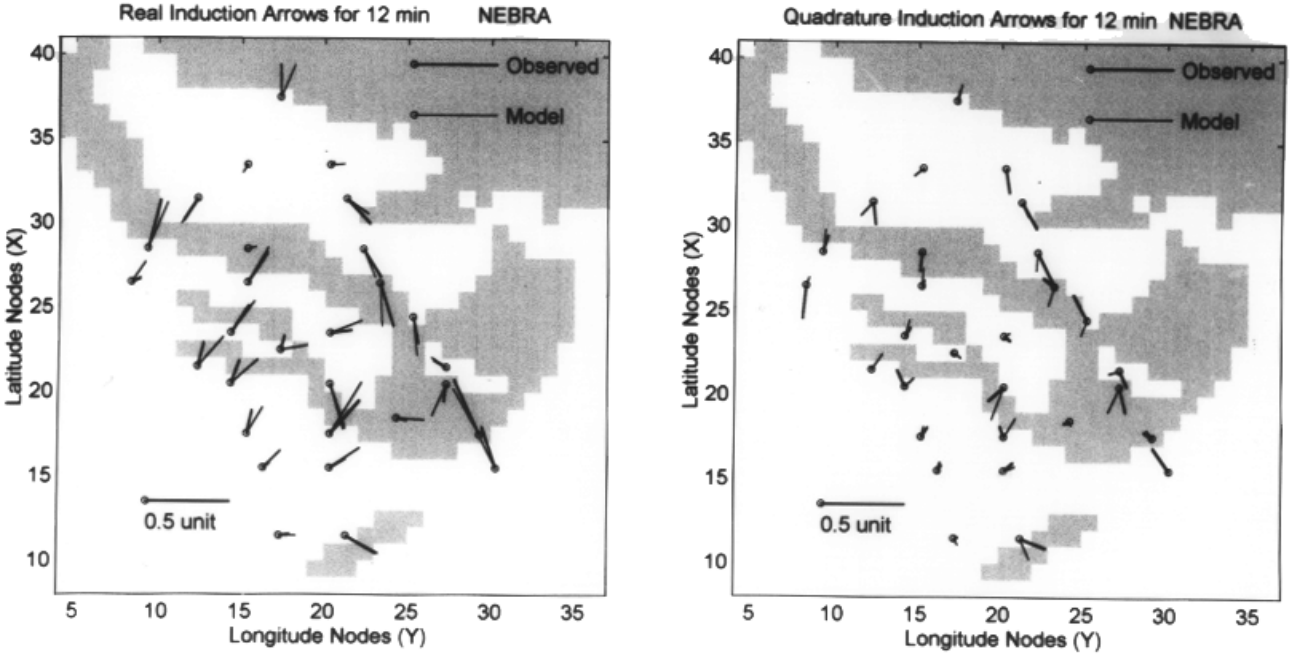

conductance zones.

part of the PBCA.

In the NW part, when the conductivity distribution in the Marajó Graben was solely guided by the isopach, the resulting induction pattern failed to reproduce the reversal of the arrows between TOM and TAI . However, when the conductivity distribution (Fig. 8) was allowed to follow the graben-like structure bounded by normal faults (shown in Fig. 1), the resulting arrow pattern reproduced the reversal between TOM and TAI (Fig. 9). The thin sheet model traces the path of this LINK anomaly and its linkage with the PBCA near stations COC-SIN (Figs. 8 and 10). The overall depth-integrated conductance of the LINK anomaly is close to 1000 S, only about half of the value estimated for the PBCA. This is consistent with the disappearance of the anomalous signatures of the LINK anomaly at longer periods.

On the central-western part of the array, a model response consistent with the observation was achieved by incorporating two narrow conductive strips, sub-parallel to the LINK anomaly (Fig. 8). The inferred conductance distribution model favors the linkage of these narrow conducting strips with the linear conducting zone on the western flank of the PBCA. Perhaps, the induction effects of these narrow strips coupled with the response of the LINK anomaly give the spatially uniform arrow pattern on the western part of the array.

A narrow NE-SW trending conductance zone, introduced in the thin sheet model to explain the behavior of the induction arrow at BAL, is aligned with the Transbrasiliano Lineament. Additionally, a little enhanced conducting zone, aligned NE-SW, was required to account for the SW pointing arrow at the station STE.

The 2-D Sheet Current Inversion

The magnetovariational response of the PBCA along the eastern profile is now inverted in terms of a steady sheet current flowing at some depth below the surface. Following closely the formulation described by Woods & Lilley (1980), the adopted inversion scheme simulated the sheet current by a finite number of current elements of infinite lengths

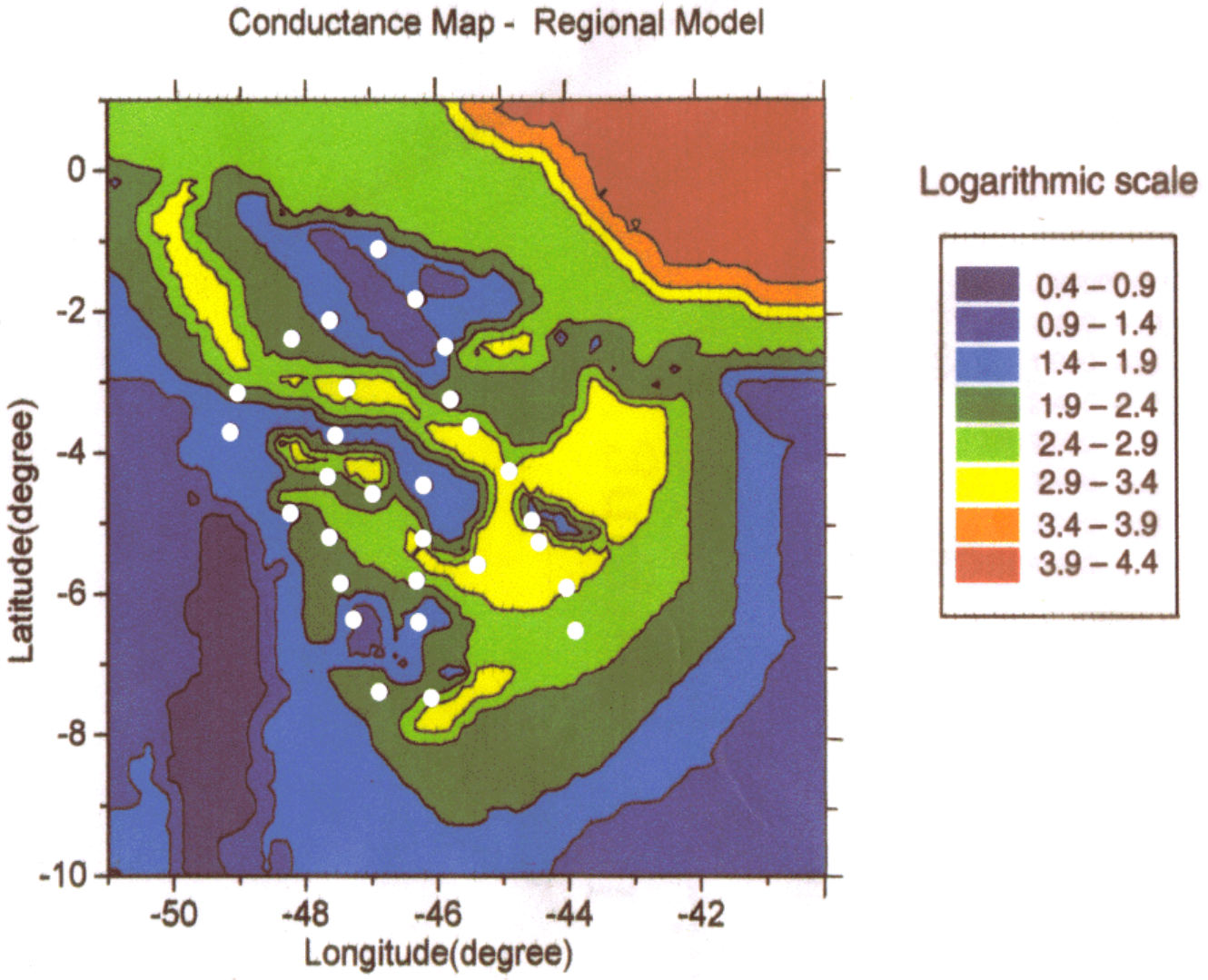

Figure 10 - The overall distribution of conductance values, in logarithmic scale, obtained from the thin sheet model.

along the strike direction. Individual current elements were represented by current bands of variable intensities. The magnetic effects above a single current element was calculated from the Bio-Savart law and the total horizontal or vertical field at any point on the surface was expressed as a linear combination of fields from all current elements. If the total number of points, at which the entire field is known, is greater than or equal to the number of current elements, then a direct matrix inversion of the field produces a current distribution in the ground.

The inversion scheme and simplifications introduced to obtain smooth and stable solutions are provided by Arora et al. (1998b). Inversion solutions were obtained using profiles of anomalous fields, both in time (Fig. 11a) and frequency (Fig. 11b) domains. The inverted current density distribution, that reproduces the observed induction response, is given in the lower panels of Fig. 11. Current inversions of the time-domain profiles were obtained by locating the model current sheet at varying depths of 5, 10 and 15 km. For the sheet located at depths greater than 10 km, the inverted current distribution requires a narrow belt with a current flow in a direction opposite to the main broad band. From the induction point of view, the existence of concurrent zones with a reversed current flow is physically implausible (Woods & Lilley, 1980), so depths greater than 10 km for the unidirectional sheet current were found to be incompatible with the observed pattern. Thus, because the sheet represents the integrated current flow in the depth range of 10 km, it is reasonable to visualize that the bulk current flow would be concentrated in the conductive sedimentary sequence of the basin in the depth range of 5 km. Based on this hypothesis, the inversion of frequency-domain profiles was carried out by placing the sheet current at the depth of 5 km (Fig. 11b). Both inversions produce current density distributions identical in their principal features. Noting this persistent behavior, Arora et al.(1998b) observed that the spatial pattern of the inverted current distribution could be geologically viewed as a graben-horst-graben structure in the basement (Fig. 12b), or more simply as a sediment filled broad graben-like feature enclosing a resistive body (Fig. 12c). This later condition can also be simulated by a conductive block intruded by a resistive zone within the central part of the basin (Fig. 12d). These models served as the initial starting models in developing a more quantitative 2-D geo-electrical model by a trial and error procedure. The inverted current distribution is also used later in this article to make a correlation with other geophysical response functions.

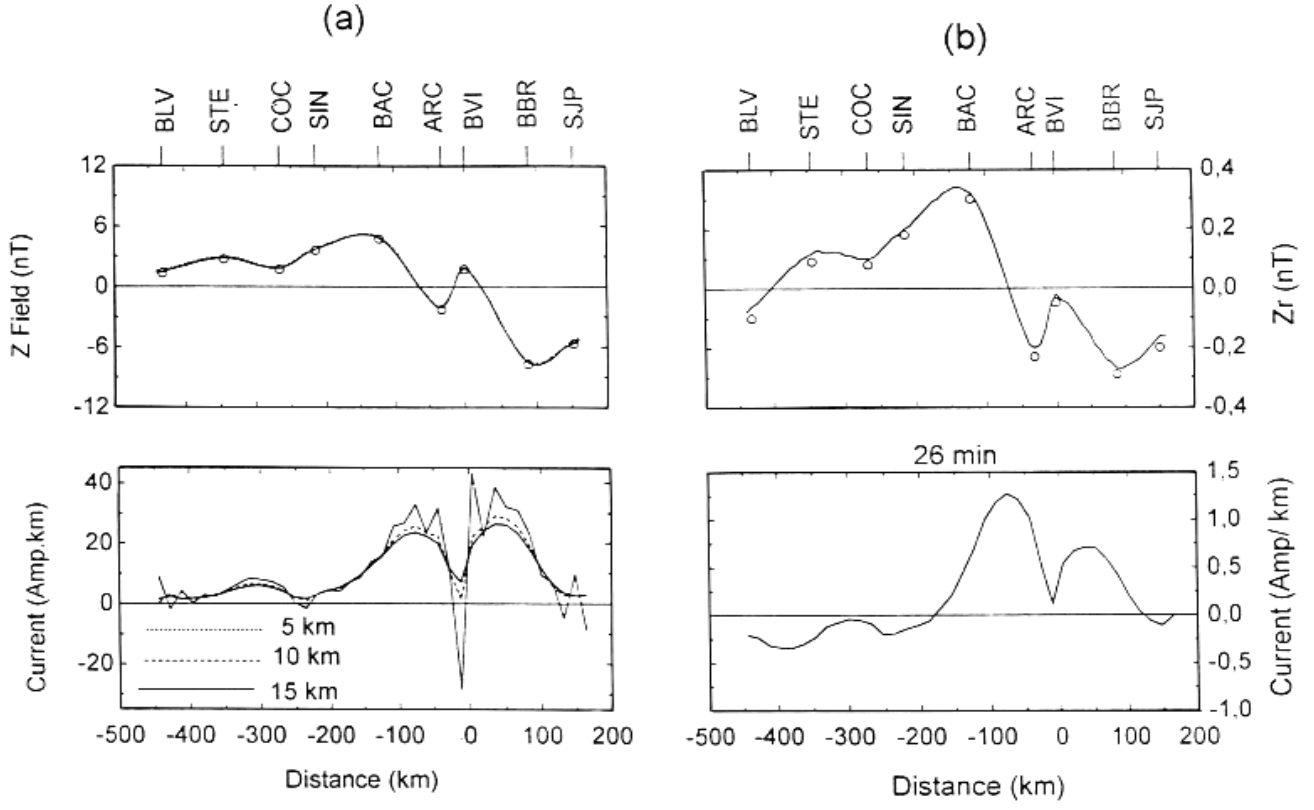

Figure 11 - Plots of anomalous vertical field (Z), along the profile AA', calculated for time and frequency domains, in the upper diagrams of (a) and (b), respectively. The lower panels give the respective inverted sheet current distributions. The inversions of the time domain field variations are obtained when the sheet current is considered to be located at variable depths of 5, 10 and 15 km, whereas the frequency domain inversion corresponds only to the depth of 5 km.

The 2-D Conductivity Model for the PBCA

In order to constrain further the structural configuration of the PBCA, in a vertical plane across the strike direction, a 2-D electrical conductivity modeling of the MV response along the profile AA' was undertaken. The conductivity distribution model that produces an induction response similar to the observed one was probed using a 2-D trial and error forward modeling approach developed by Cerv et al. (1987). The numerical scheme permits the simulation of quite complex conductive structures by a grid of variable horizontal and vertical mesh. This procedure facilitated the transformation of the geological cross-section of the basin (Fig. 12a) into an electrical section composed by simple step structures (lower panels of Figs. 13 and 14). The assignment of resistivity values was again governed by the MT soundings. The two upper layers of the electrical section, obtained from the 1-D interpretation of the MT sounding (Fig. 6b) for the exposed Jurassic-Cretaceous formations and underlying Balsas Group, were assigned resistivities of 50 Ω.m and 10 Ω.m, respectively. The underlying Paleozoic sedimentary sequence, represented jointly by the Serra Grande and Canindé Groups, was characterized by the resistivity of 7 Ω.m, in agreement with the extensive MT surveys in the adjoining Paraná Basin (Stanley et al.,1985).

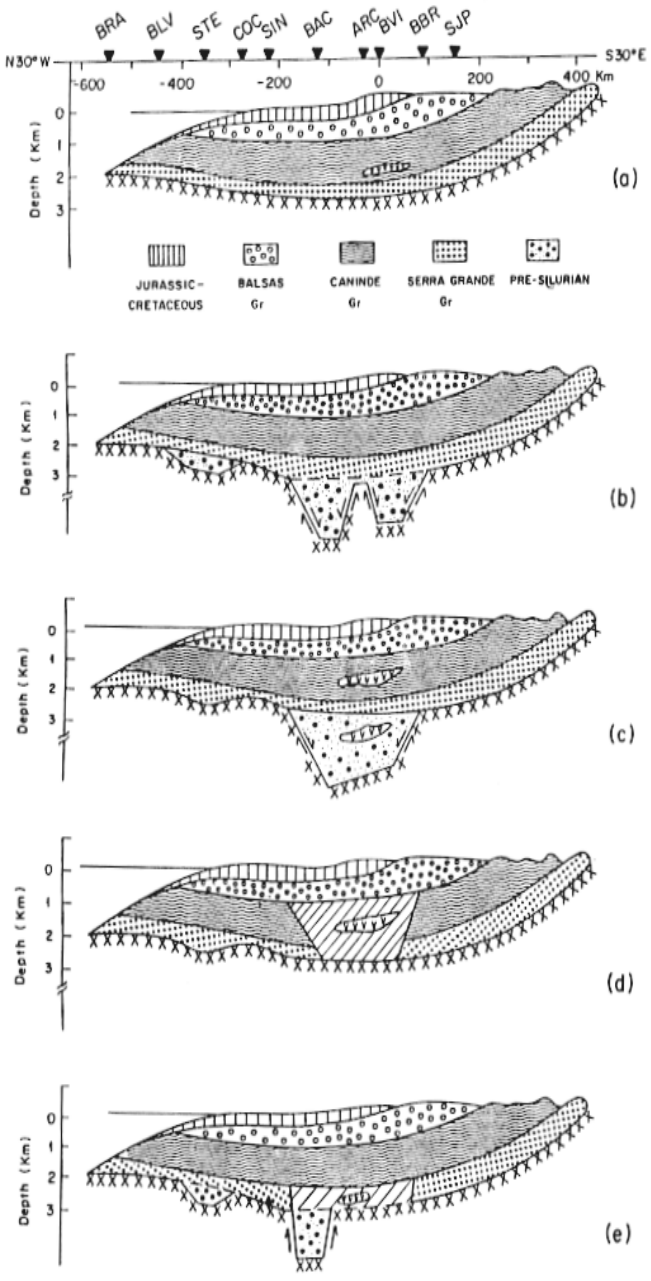

Figure 12 - Schematic geological cross-sections of the Parnaíba basin obtained along the line BB' (marked on Fig.1): (a) cross-section based on outcrops and exploratory wells (adapted from Caputo & Lima, 1984); (b), (c), and (d) cross-section options based on the inverted sheet current distribution for a depth of 5 km, shown in the lower panels of Fig.11; (e) final PBCA model, based on the deduced 2-D electrical conductivity distribution model, as shown in the lower panel of Fig.13.

Owing to the well-known problem of non-uniqueness associated with forward modeling technique, the range of numerically tested models was restricted by the information provided by the sheet current inversion. The oceanic coast effect in the electrical models probed was simulated by introducing a conductive sheet extending seaward from the surface position of the coastline on the NW end of the profile. Further, consistent with the MT sounding near the central part of the Parnaíba Basin, the source of the anomalous conductivity in the geo-electrical model was considered to be seated in the deeper parts of the basin (Fig. 13). The lateral, vertical extent, and the resistivity values of the block(s) in the deeper parts were adjusted in a trial and error process to find a match to the observations. The attempt was to find the model that could satisfy the observed response at a wide range of periods. This requirement greatly restricted the range of qualifying models. For example, conductive structures, with well-defined geometry beneath the central part of the basin, in conjunction with the oceanic layer, could satisfactorily reproduce the spatial characteristics of the response observed at the 12 minutes period. However, such model would fail to reproduce all the features of the observed response at the longer periods of 26 and 43 minutes (dashed curves in Fig. 13).

In fact, the level of misfit appears to become worse at increasingly longer period, on the NW flank of the profile. When an additional extended conducting slab was introduced at depth in the oceanic part of the profile, the revised response (solid curve) was accountable for the observed response at all periods. The Z_r values on the NW corner of the pseudo-section (Fig. 5) attain largest values at longer periods above one-hour, rather than at the shortest periods. The inclusion of a conducting slab at depth on the oceanic side of the coastline, in addition to the conducting seawater, is consistent with this behavior of the Z_r. Of the several tens of models investigated, the one qualifying model that largely reproduced the spatial as well as the period dependence of the observed response is shown in Fig. 13. The comparison of the observed and calculated response at three

representative periods is also shown.

The overall picture of the mapped conductive zone (hatched area) can be viewed as an ensemble of three blocks; (i) a roughly 240 km wide tabular block within the deeper central part of the basin, (ii) a localized highly resistive (700 W.m) block embedded in the above central conductive block, and (iii) a narrow sediment filled graben-like structure extending into the basement. The central block with a resistivity of less than 1 W.m accounts for the long wavelength anomaly pattern with minimum/maximum near stations COC-SIN and BBR. The induction responses of the graben-like structure and intrusive resistive body, respectively, produce the sharp rise of the MV response between BAC and ARC and introduce a short wavelength anomaly between ARC and BVI. The combined induction response of these blocks is able to account for the spatial characteristics of the observed response at various periods (Fig.l3b). Some further numerical experimentation showed that a resistivity of less than 1 W m was essential to account for the frequency (period) dependence as well as to produce the short wavelength anomaly by the presence of an intrusive

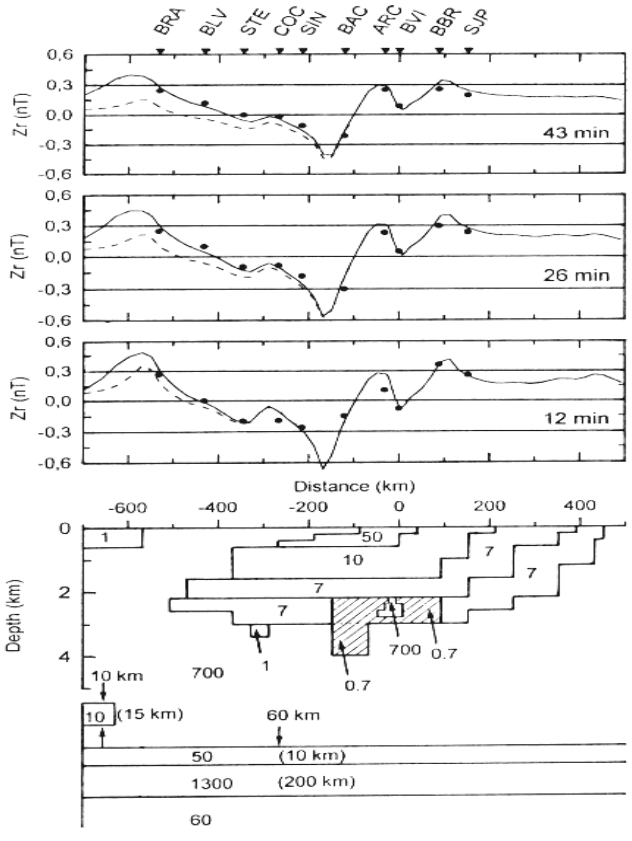

for the PBCA, along the AA' profile. The hatched area marks a high conductivity zone with an intruded resistive block. The values included in the different blocks denote electrical resistivity in W.m. The upper three profiles compare the observed (solid circles) and the calculated response of the geo-electrical model (continuous lines) at the three indicated periods. The broken curves show the calculated response when a deeper conductive oceanic slab, shown in the left side of the lower diagram, is not considered.

resistive body. The presence of an anomalous conducting horizon within the main body of the basin is unequivocally detected by MT surveys (Oliveira & Fontes, 1991). This 2-D geo-electrical model is used to update the geological/ structural cross-section of the Parnaíba Basin in Fig. l2e.

THE SOURCE OF THE ENHANCED CONDUCTIVITY IN THE CENTRAL PART OF THE BASIN

Moderately raised conductivity values, commonly found in sedimentary environments, are often explained by electrolitic conduction through sedimentary rocks, in contrast to the resistive crystalline basement. However, the likely mechanisms responsible for the anomalously high conductivity detected in the deeper central part of the basin are very elusive. The generation of high conductivity, of the order of 1 S/m, by ionic conduction through an extensive interconnected network of saline filled pores would require porosity values higher than 12 per cent (Jones & Craven, 1990). They are very high values to sustain for the required long period of time, or even in a primordial basin environment. Furthermore, the presence of very saline fluids or of a thick sequence of black shales, another probable candidate, has not been detected on deep wells, yet these wells are not in the area of the anomalies.

Nevertheless, the correspondence of the zones of high conductivity with the regions of Mesozoic magmatism seems to indicate a probable causal relationship between the two phenomena. Hydrous fluids released during the re-crystallization of the magmatic intrusions could contribute to the enhanced conductivity of the sediments (Stanley et al., 1990). It also seems plausible that the anomalous conductivity, pervasive on a large region, might have been thermally enhanced, in association with the magmatic event. Laboratory measurements by Bucha (1980) have shown that when hydrocarbon-saturated sediments are heated above the temperature of 200° C, carbon films are produced by pyrolysis reactions associated with diagenesis. The presence of interconnected carbon films can enhance the conductivity of the medium. Apart from the generation of carbon films, the pyrolysis reaction was also shown to produce secondary magnetite that could produce concurrent anomalies in a magnetic data. The existence of an apparent relationship between conductivity and magnetic anomalies was reported by Bucha (1980), in studies of the outer flysch belt around the Carpathians mountain range. Similarly, Duba et al. (1988) have illustrated the case where light hydrocarbons would be driven off or destroyed during diagenesis.

Fig. l4 gives the total magnetic intensity (IGRF removed) anomaly map of the Parnaíba Basin, based on aeromagnetic data collected by Petrobras. The outline of the high conductance zones (PBCA and LINK anomaly) as mapped by the thin sheet model has been superimposed. The broad magnetic high in the north, associated with the continental margin, and the almost continuous, yet narrower, NE trending magnetic high overlying the regional

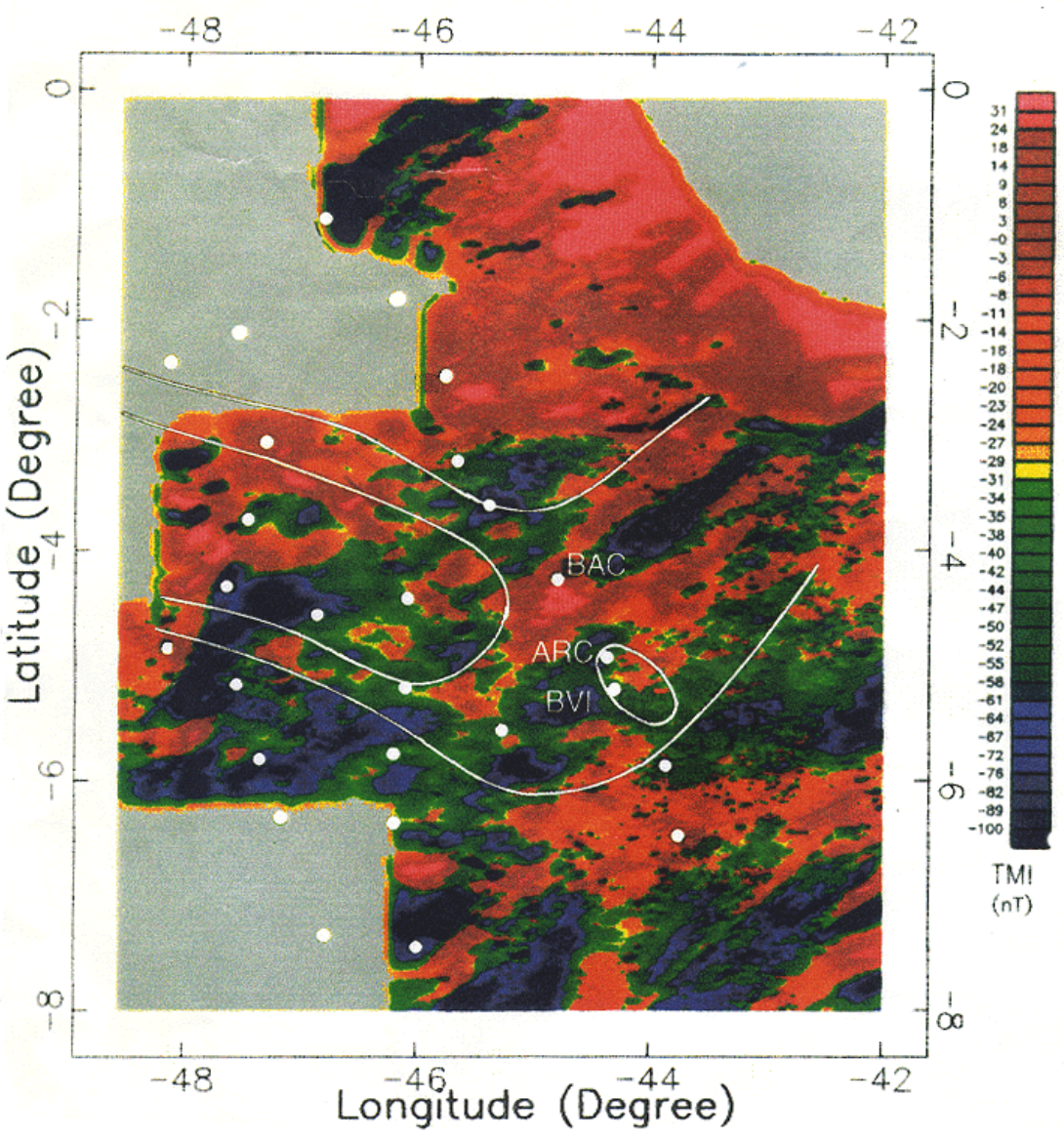

Figure 14 – Illustration of the total field aeromagnetic anomaly map overlain by the high conductance zone (PBCA and LINK anomaly) mapped in the present study. The magnetometer site locations and respective code names are also shown.

Transbrasiliano Lineament tend to dominate the magnetic anomaly map. In the intervening region of these two prominent features, the magnetic anomaly pattern is characterized by a sequence of NE trending highs that, beginning from the central part of the basin, stretch towards the northeast and enclose many scattered lows. It is to be noted that the high density aeromagnetic data provide a much more detailed picture of the sub-surface configuration than that permitted by the conductance distribution map (Fig. 10), deduced from widely spaced magnetometers. Given allowance for this difference in the resolution of the two maps, the broad magnetic high, in respect to the orientation and spatial extent, tends to outline the high conductance PBCA zone. It is noteworthy that an intense magnetic high, centred between stations BAC and ARC, coincides with the location of the graben-like structure mapped by the 2-D model. Further, the surface location of the intruded resistive body in the 2-D model is marked by a magnetic low. Also in the northwestern part, the LINK anomaly, with some offset, aligns with magnetic highs which on this part preferentially strike in the NW direction. The apparent crude correlation between conductive and magnetic signatures tend to suggest a common source mechanism, such as the simultaneous generation of carbon and magnetite by pyrolysis reaction triggered by magmatic thermal events. However, quantitative interpretation of magnetic anomalies would help to establish the structural and physical relationship between the conductivity and magnetic anomalies.

GEOLOGIC AND TECTONIC IMPLICATIONS OF THE MAPPED CONDUCTIVE ZONES IN THE EVOLUTION OF THE BASIN

The regional pattern of the conductivity distribution (Fig. 10) suggests a complex structural configuration although, in the surface, the Parnaíba Basin presents a simple quasi-elliptical distribution of the geological units. The two main anomalies (PBCA and LINK) fall in a region where no well reached the basement. According to a basement map from Cordani et al. (1984), the anomalous area would cross the Gurupi fold belt and a postulated internal cratonic block, underneath the sediments, in the center of the basin.

The most dominant conductivity feature (PBCA) is marked by a NE-SW trend that coincides with the projection of the Grajaú Fault line, on the western side. On the eastern side of the anomaly, the trend coincides with the land ward projection of the Parnaíba River Lineament. The parallelism of this trend with the Transbrasiliano Lineament suggests a control of the NE-SW oriented tectonic elements on the evolution of this portion of the Parnaíba basin from early stages. The results also indicate that the NE-SW features are present much further west than the currently mapped lineament. The 2-D numerical model has approximated the structural configuration of the PBCA as a graben-like structure in the basement and a tabular high conductivity block confined to the central part of the basin with an embedded resistive body. While the existence of a wide conducting block confined to the central part of the basin is consistent with the magnetotelluric data, the graben-like structure in the basement is corroborated by the aeromagnetometric data.

Furthermore, the development of graben structures as precursors to the subsidence of the Parnaíba basin has been suggested by many researchers based on interpretations from geological and geophysical data (Brito Neves et al., 1984; Cunha, 1986; Góes et al., 1990). Nunes (1993) has inferred a series of isolated basement grabens of Proterozoic age in the PBCA area, yet with NW-SE trends. Nevertheless, the graben structures probably formed depositional sites for the pre-Serra Grande volcanic-sedimentary sequences. Also, the narrow elongated conductive belt mapped on the western flank of the PBCA (Fig. 10), perhaps marks another graben where pre-Serra Grande sediments have been preserved. In the region of the Transbrasiliano Lineament, the existence of graben-like structures with sediments possibly older than the Serra Grande Group, has been inferred from MT and gravity data (Sousa & Oliveira, 1995).

The positional correspondence of the broad PBCA and the elongated LINK anomaly with zones of major Cretaceous magmatism suggests the occurrence of channeled activities, in part, along pre-existing basement structures possibly associated with the PBCA and LINK anomalies. In this tectonic scenario, the resistive body found embedded in the conductive host within the central block of the basin may be interpreted as an intrusive body. A number of wells have indeed detected the presence of a large number of intrusive bodies in the basin (Mesner & Wooldridge, 1964). The present study, however, provides evidence on the possible dimension of these intrusive bodies.

The smaller Southern Structure anomaly, based on results from the BAL station, roughly coincides with a large area where several deep wells reached immature sediments beneath the Serra Grande, southeastern of the widespread Jurassic eruptives (Cordani et al., 1984; Cunha, 1986).

The Bouguer map shown on Fig. 15 presents two elongated gravity lows with amplitudes from -50 to -100 mGal trending in the N-S direction, parallel to the Araguaia-Tocantins fold belt in the western side, and in the NE-SW direction, in the eastern side, partly enclosing the Transbrasiliano Lineament. They form a slanted V pattern with the lower tip positioned near the Southern anomaly. Góes et al. (1990, 1993) have indicated that the geographic area of the V shaped gravity anomaly coincides with a zone of Cambro-Ordovician, Middle Proterozoic, and Late Proterozoic graben-like structures. Except for the Southern Structure, the western portions of the E-W trending LINK and of the narrower parallel conductive belt below the LINK anomaly, the other magnetometer stations of the western array profile (Fig. 1) failed to indicate a major western N-S conductive anomaly, coincidental with the western branch of the gravity low.

Sousa (1995), however, has suggested that an anomalous dense material placed at mid-crust depths would account for the observed regional gravity anomaly. In this case, the inference of underplating related to extensional processes does not conflict with the above suggested thermal pulse responsible for the conductive anomalies.

The overall inferred conductivity distribution also provides geophysical evidence on the possible direction of sea connections during the geological evolution of the basin. The induction arrows at TOM and TAI in the NW corner (Fig. 3), despite their favorable locations, do not point towards the Marajó Graben, where sediments, largely of Mesozoic and Cenozoic age, present a thickness of about 6 km. Instead, the arrow pattern indicates a structure running between them and striking N60^{o}W. In fact, the structure causing this concentration of induced currents appears to be aligned with mapped fault lines within the Marajó region (Fig.1). The continuation of the conducting path along the LINK anomaly may be seen as a prolongation of this structure underneath the Parnaíba Basin. In such a scenario, the LINK anomaly may be seen as relics of a sedimentary channel which might have acted as a pathway for sea transgressions and would have connected the Amazon Basin with the Parnaíba Basin through the Marajó region.

The linkage of the Marajó and Parnaíba regions is independently corroborated by the gravity Bouguer anomaly map (Sousa, 1996) shown in Fig. 15. Composed by low density sediments, the Marajó region is marked by a pronounced gravity low, whose center corresponds to the thickest column of sediments. Further southeast of the

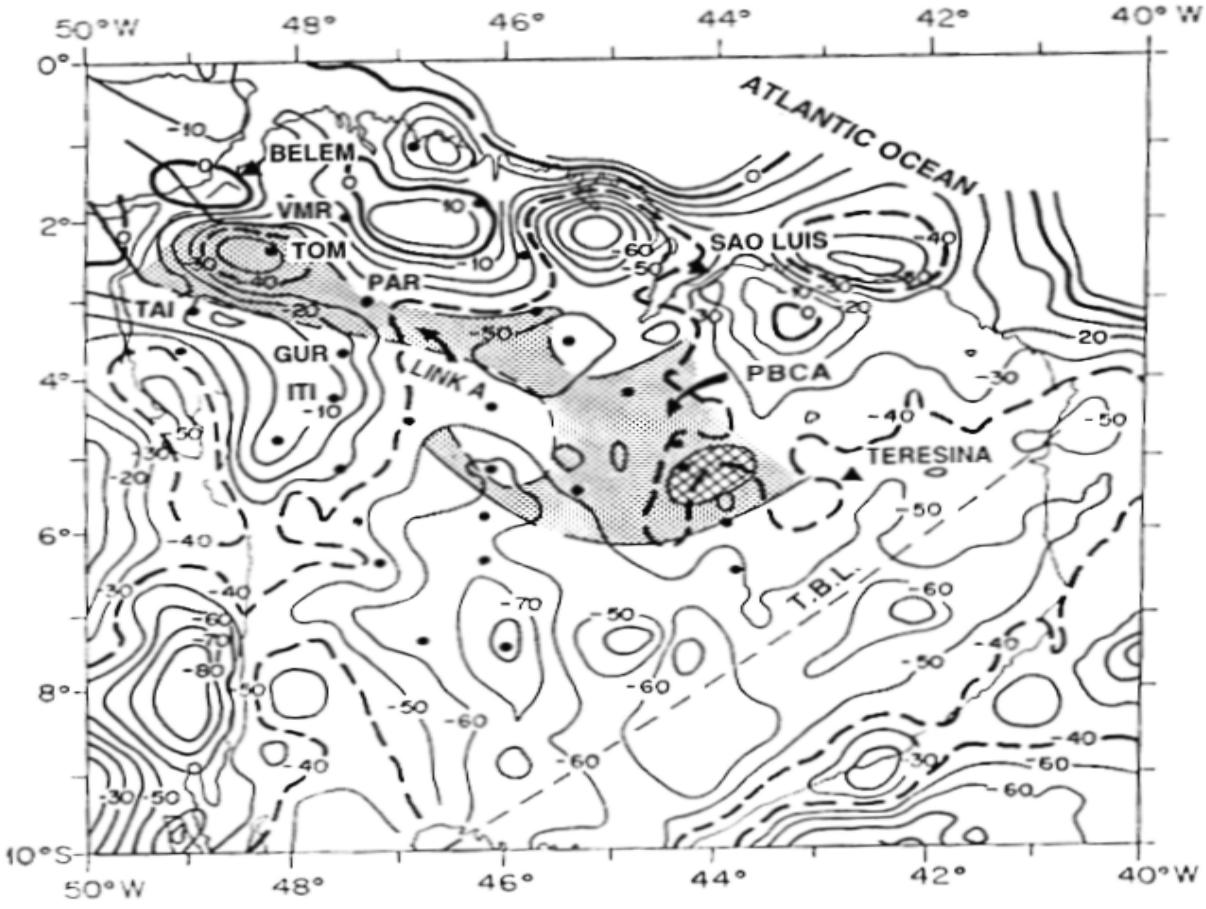

Figure 15 – Bouguer anomaly map (adapted from Sousa, 1993) overlain by the high conductive zone mapped by the present study.

Marajó Graben, the region of the Arch of Tocantins is characterized by a gravity high with a dividing low. The TAI, GUR and ITI stations are over the southwestern high, VMR is over the northeastern high, and TOM and PAR are located within the dividing low. The axis of the gravity low, beginning in the Marajó region and passing through the gravity low located between the gravity highs overlying the Arch of Tocantins, traces the path of the high conductivity zone (LINK anomaly). On the hypothesis that the gravity low implies the occurrence of a thicker sequence of sediments relative to the gravity high, an enhanced concentration or channeling of the currents in the sediments could explain the correlation of the gravity low with the conductivity high.

This connectivity also permits to infer that, during a certain phase of the geological evolution, the geographical extent of the seawater was much more ample and had crossed over the Arch of Tocantins. In this line of reasoning, the position of the LINK-PBCA anomaly is in agreement with the suggested seawater connections, by Cunha (1986), of the Parnaíba region with the basins located in the west and east, respectively, of the São Luis-Western Africa Craton, in the Gondwana continent.

CONCLUSIONS

The efficacy of the GDS in providing the regional picture of the internal electrical conductivity distribution has been documented in the context of the intracratonic Parnaíba Basin. In contrast to the simple oval shaped configuration of the surface geoloy, the inferred conductivity distribution is marked by well-defined patterns probably reflecting the trends of the basement structures.

The most dominant feature is a NE-SW high conductive belt (PBCA) in the east-southeast portion of the basin, whereas the second prominent trend runs NW-SE (LINK) from the Marajó Graben to the Parnaíba Basin. The NE-SW trending anomaly in the east-southeastern part of the basin could be ascribed to tectonic events associated with the Transbrasiliano Lineament, in the early evolution of the basin. The transverse LINK anomaly probably demarcates a basement structure that has preserved sediments from sea instructions from the Marajó during some of the early stages of the basin evolution.

The deduced picture of conductivity distribution in the vertical plane across the PBCA provides evidence on the presence of a graben-like structure in the basement. This is consistent with the aeromagnetometric data. The modeled

graben-like structure appears to have influenced the nature of sedimentation in the initial stages of the basin evolution and could have served as likely conduits for the extrusion of the magma during the Cretaceous magmatic activities.

The presented evidence that sediments in the deeper central part of the basin are characterized by an anomalous high conductivity is corroborated by magnetotelluric measurements. The issue of the generating mechanism of the measured highly enhanced condutivity is not solvable by GDS technique alone. Yet, noting the correspondence of the mapped high conductivity zone with the areas of intense Cretaceous magmatic activities, it has been suggested that the sediments may owe the anomalous high conductivity to interconnected carbon films produced from the pyrolysis of pre-existing hydrocarbon satured sediments. Given that the pyrolysis reaction is also expected to produce secondary magnetite, a search for coincidental signature in the aeromagnetometric data may be the key to a positive identification of the source of the high conductivity zone. In view of the fact that the correct appraisal of the likely source of the high conductivity has important implications on the evaluation of hydrocarbon prospects in the basin, the interpretation of aeromagnetometric data may be rewarding. The indication of another zone of anomalous high conductivity, south of the array, shows the necessity of an expanded array with more magnetometers covering the entire area of the basin. Furthermore, magnetotelluric measurements along closely spaced profile across the PBCA would provide a better depth resolution as well as a more precise estimate of the formation resistivity values.

ACKNOWLEDGMENTS

We are grateful to Alícia L. C. Gonzales Alarcon for conducting the reviewing process, to F. E. M. (Ted) Lilley and Igor I. G. Pacca for their constructive suggestions as journal reviewers. The work was suported in part by research funds from FAPESP (Fundação de Amparo à Pesquisas do Estado de S.Paulo) (Project nº. 93/0652-2) and CNPq (Conselho Nacional de Desenvolvimento Científico e Tecnológico) (Project nº.522342/94-9) and by Fellowships awarded by CNPq.

REFERENCES

ADAM, A. -1997- Interpretation of the electrical conductivity anomalies in the continental lithosphere. In Natural source electromagnetic induction in the Earth (B.R. Arora & Sri Niwas, eds.), New Age International (P) Limited Publishers, New Delhi, 197-250.

AGARWAL, A. K. & WEAVER, J. T. -1990- A three-dimensional numerical study of induction in southern India by an electrojet source. Phys. Earth Planet. Inter., **60**: 1-17.

ALMEIDA, F. F. M. DE, HASUI, Y., BRITO NEVES, B. B. DE & FUCK, R. A. -1981- Brazilian structural provinces: an introduction. Earth Sci. Rev., **17**: 1-29.

ARORA, B. R. -1997- Geomagnetic deep sounding. In Natural source electromagnetic induction in the Earth (B. R. Arora & Sriniwas, eds.), New Age International (P) Limited Publishers, New Delhi, 80-128.

ARORA, B. R., RIGOTI, A., VITORELLO, I., PADILHA, A. L., TRIVEDI, N. B. & CHAMALAUN, F.H. -1997- Electrical imaging of the intracratonic Parnaíba basin, north-northeast Brazil. J. Geomagn. Geoelectr., **49**: 1631-1648.

ARORA, B. R., RIGOTI, A.,VITORELLO, I., PADILHA, A. L., TRIVEDI, N. B. & CHAMALAUN, F.H. -1998a- Magnetometer array study in north-northeast Brazil: conductive image building and functional induction modes. Pure Appl. Geophys., **152**: 349-375.

ARORA, B. R., VITORELLO, I., PADILHA, A. L., TRIVEDI, N. B., RIGOTI, A. & CHAMALAUN, F.H. -1998b- Geological interpretation of the Parnaíba basin magnetovariational anomaly using a 2-D sheet current inversion. Acta. Geod. Geoph. Hung., **33**: 167-155.

ARORA, B. R., PADILHA, A. L., VITORELLO, I., TRIVEDI, N. B., FONTES, S. L., RIGOTI, A. & CHAMALAUN, F. H. -1999- 2-D geoelectrical model for the Parnaiba Basin conductivity anomaly, North-northeast Brazil and its tectonic implications. Tectonophysics, **302**: 57-69

BAILEY, R. C., EDWARDS, R. N., GARLAND, G. D. & GREENHOUSE, J. P. -1974- Electrical conductivity studies over a tectonically active area in eastern Canada. J. Geomagn. Geoelectr., **26**: 125-146.

BANKS, R. J. -1979- The use of equivalent current systems in the interpretation of geomagnetic deep sounding data. Geophys. J.R. Astr. Soc., **56**: 139-157.

BANKS, R. J. -1986- The interpretation of the Northumberland Trough geomagnetic variation anomaly using two-dimensional current models. Geophys. J. R. Astr. Soc., **87**: 595-616.

BANKS, R. J., IRVING, A. A. K. & LIVELYBROOKS, D.W. -1993- The simulation of magnetic variation anomalies using single-station data. Phys. Earth Planet. Inter., **81**: 85-98.

BANKS, R. J., LIVELYBROOKS, D., JONES, P. & LONGSTAFF, R. -1996- Causes of high conductivity beneath the Iapetus suture zone in Great Britain. Geophys. J. Int., **124**: 433-455.

BEAMISH, D. -1977- The mapping of induced currents around the Kenya rift: A comparison of techniques. Geophys. J.R. Astron. Soc., **50**: 311-332.

BEAMISH, D. & BANKS, R. J. -1983- Geomagnetic variation anomalies in northern England: processing and presentation of data from a non-simultaneous array. Geophys. J.R. Astron. Soc., **75**: 513-539.

BIGARELLA, J. J. -1973- Geology of the Amazon and Parnaíba basins. In The Ocean Basins and Margins, Vol. 1- The South Atlantic (A.E.M. Nairn & F.G. Stehli, eds.), Plenum Press, New York, 25-86.

BRITO NEVES, B. B., FUCK, R. A., CORDANI, U. G. & THOMAZ, A. -1984- Influence of basement structures on the evolution of the major sedimentary basins of Brazil: a case of tectonic heritage. J. Geodynamics, **1**: 495-510.

BUCHA, V. -1980- Geomagnetism of the external flysch Czechoslovakian Carpathians and the possible causes of the anomalous geophysical manifestations. Stud. Geophys. Geod., **24**: 227-251.

CAPUTO, M. V. & LIMA, E. C. -1984- Estratigrafia, idade e correlação do grupo Serra Grande- Bacia do Parnaíba. Anais XXXIII Congresso Brasileiro de Geologia, 740-752, Rio de Janeiro, RJ.

CERV, P., PEK, J. & PRAUS, O. -1987- Numerical modelling of geoelectrical structures in Czechoslovakia. Phys. Earth Planet. Int., **45**: 170-178.

CHAMALAUN, F. M. & BARTON, C. E. -1993- The large scale electrical conductivity structure of Australia. J.Geomagn. Geoelectr., **45**: 100-121.

CHAMALAUN, F. H. & McKNIGHT, J. D. -1993- A New Zealand wide magnetometer array study. J. Geomagn Geoelectr., **45**: 741-759.

CHAMALAUN, F. H. & WALKER, R. -1982- A microprocessor based digital fluxgate magnetometer for geomagnetic deep sounding studies. J. Geomagn. Geoelectr., **34**: 491-507.

CHANDRASEKHAR, E. & ARORA, B. R. -1994- On the source field geometry and geomagnetic induction in southern India. J Geomagn. Geoelectr., **46**: 815-825.

CONDANI, U. G., NEVES, B. B., FUCK, R. A., PORTO, R., THOMAZ FILHO, A. & CUNHA, F. M. B. -1984- Estudo preliminar de integração do Pré-cambriano com os eventos tectônicos das bacias sedimentares Brasileiras. Petrobras, Cenpes, Sintep III, série ciência-técnica-Petróleo, **15**, 70 pp.

CUNHA, F. M. B. -1986- Evolução paleozóica da Bacia do Parnaíba e seu arcabouço tectônico. M.Sc. thesis, Univ. Federal Rio de Janeiro, Inst. Geociências, Rio de Janeiro, Brazil

DNPM (Departamento Nacional da Produção Mineral), -1971-. Mapa tectônico do Brasil 1:5,000,000.

DUBA, A. L., HUENGES, E., NOVER, G. & WILL, G. -1988- Impedance of black shale from the Munsterland 1 borehole: an anomalously good conductor? Geophys. J. Int., **94**: 413-419.

EGBERT, G. D. & BOOKER, J. R. -1986- Robust estimation of geomagnetic transfer functions. Geophys. J. R. Astron. Soc., **87**: 173-194.

EVERETT, J. E. & HYNDMAN, R. D. -1967- Geomagnetic variations and electrical conductivity structures in south-western Australia. Phys. Earth Planet. Inter., **1**: 24-34.

GÓES, A. M. O. & FEIJÓ, F.J. -1994- Bacia do Parnaíba. B. Geociências, PETROBRAS, **8(1)**: 57-67.

GÓES, A. M. O., SOUZA, J. M. P. & TEIXEIRA, L. B. -1990- Estágio exploratório e perspectivas petrolíferas da bacia do Parnaíba. B.Geociências, PETROBRAS, **4(1)**, 55-64.

GÓES, A. M. O., TRAVASSOS, W. A. S. & NUNES, K. C. -1993- Projeto Parnaíba: Reavaliação da bacia e perspectivas exploratórias. Relatório Interno PETROBRAS.

GOUGH, D. I. & INGHAM, M. R. -1983- Interpretation methods for magnetometer arrays. Rev. Geophys. Space Phys., **21**: 805-827.

GOUGH, D. I., McELHINNY M. W. & LILLEY, F. E. M., -1974- A magnetometer array study in southern Australia. Geophys. J.R. Astr. Soc., **36**: 345-362.

GOUGH, D. I., McKIRDY, D. M., WOODS, D. V. & GEIGER, H. -1989- Conductive structures and tectonics beneath the EMSLAB land array. J.Geophys.Res., **94**: 14099-14110.

GREGORI, G. P. & LANZEROTTI, L. J. -1980- Geomagnetic depth sounding by induction arrow representation: a review. Rev. Geophys. Space Phys., **18**: 203-209.

JONES, A.G. & CRAVEN, J.A. -1990- The North American Central Plains conductivity anomaly and its correlation with gravity, magnetic, seismic and heat flow data in Saskatchewan, Canada. Phys. Earth and Planet. Inter., **60**: 169-194.

LIMA, J. P. R. , OLIVEIRA, M. F. B., FONTES, S. L. & MEJU, M. A. -1996- Evidência do lineamento Transbrasiliano na bacia do Parnaíba utilizando o método magnetotelúrico. Proc. XXXIX Brazilian Geological Congress. **2**: 372-375. Salvador, BA, Brazil.

McKIRDY, D. M., WEAVER, J. T. & DAWSON, T. W. -1985- Induction in a thin sheet of variable conductance at the surface of the stratified Earth- II: three-dimensional theory. Geophys. J.R. Astron. Soc., **80**: 177-194.

MENVIELLE, M., ROSSIGNOL, J. C. & TARITS, P. -1982- The coast effect in terms of deviated electric currents: a numerical study. Phys. Earth Planet. Inter., **28**: 118-128.

MESNER, J. C. & WOOLDRIDGE, L. C. -1964- Maranhão Paleozoic basin and Cretaceous coastal basins, North Brazil. Bull. Am. Assoc. Petr. Geol., **48**: 1475-1512.

NUNES, K. C. -1993- Interpretação integrada da Bacia do Parnaíba, com enfase nos dados aeromagnéticos. Proc. 3rd International Congress of the Brazilian Geophys. Society, **1**: 152-157. Rio de Janeiro, Brazil.

OLIVEIRA, M. F. B. & FONTES, S.L. -1991- Magnetotelúrica na Bacia do Parnaíba, Primeiros resultados. Proc. 2nd International Congress of the Brazilian Geophys. Soc., **1**: 294-299, Salvador, BA,

Brazil.

ONWUMECHILI, C. A. -1967- Geomagnetic variations in the equatorial zone. Physics of the Geomagnetic Phenomena, chapter III-2 (Matsushita & Campbell, eds.), Academic Press, New York, 425-507.

PADILHA, A. L., VITORELO, I, RIGO, L. -1997- Effects of the Equatorial Electrojet on magnetotelluric surveys: Field results from northeast Brazil. Geophys. Res. Lett, **24** (1): 89-92.

PARKINSON, W. D. -1983- Introduction to geomagnetism. Scottish Academic Press, Edinburg & London.

PARKINSON, W. D. -1989- The analysis of single site induction data. Phys. Earth Planet. Inter., **53**: 360-364.

RAO, D. R. K. -1997- Geomagnetic transient variations. In Natural source electromagnetic induction in the Earth. (B. R. Arora & Sri Niwas, eds.), New Age International (P) Limited, Publishers, New Delhi, 9-47.

RIGOTI, A. -1994- Geomagnetic array study of the EEJ in NE Brazil. Ph.D. Thesis, Flinders University of South Australia, 180pp.

ROKITYANSKY, I. I. -1982- Geoelectromagnetic investigations of the Earth's crust and mantle. Springer Verlag, Berlin, 381pp.

SCHMUCKER, U. -1969- Conductivity anomalies with special reference to the Andes. In Applications of modern physics to the Earth and Planetary Interiors (S.K. Runcon ed.), Interscience, New York, pp 125-135.

SCHMUCKER, U. -1970- Anomalies of geomagnetic variations in the southwestern United States. Bull. Scripps. Inst. Oceanogr., **13**: 1-165.

SOUSA, M. A. -1995- Regional gravity interpretation of Parnaíba basin, Northern Brazil. Proc. 4th International Congress of the Brazilian Geophys. Soc., **1**: 184-187, Rio de Janeiro, Brazil.

SOUSA, M. A. -1996- Regional gravity modelling and geohistory of the Parnaíba basin (NE Brazil). Ph.D. thesis, Univ Newcastle upon Tyne, England., 127pp.

SOUSA, M. A. & OLIVEIRA, M.F.B. -1995- Geophysical evidences of the Transbrasiliano lineament in the Parnaíba basin. Proceeding 5th Simpósio Nacional de Estudos Tectónicos, **1**: 260-263, Gramado, Rio Grande do Sul.

SRI NIWAS -1997- Inversion of natural field EM data. In Natural source electromagnetic induction in the Earth, (B. R. Arora & Sri Niwas, eds.), New Age International (P) Limited, Publishers, New Delhi, 182-198.

STANLEY, W. D., SAAD, A. R. & OHOFUGI, W. -1985- Regional magnetotelluric surveys in hydrocarbon exploration. Paraná Basin, Brazil. Bull. Am. Assoc. Petro.Geol., **69**: 346-360.

STANLEY, W. D., MOONEY, W. D. & FUIS, G. S. -1990- Deep crustal structure of the Cascade range and surrounding region from seismic refraction and magnetotelluric data. J. Geophys. Res., **95**: 19419-19438.

STOERZEL, A. -1996- Estimation of transfer functions from magnetic variations of the equatorial electrojet-A method to determine static shifts in magnetotelluric data from equatorial latitudes. J. Geophysical Res., **101**: 17917-17926.

TRIVEDI, N. B., ARORA, B. R., PADILHA, A. L., DA COSTA, J. M., DUTRA, S.L.G., CHAMALAUN, F. H. & RIGOTI, A. -1997- Global Pc5 geomagnetic pulsations of March 24, 1991 as observed along the American sector, Geophys. Res. Lett., **24**: 1683-1686.

VASSEUR, G. & WEIDELT, P. -1977- Bimodal electromagnetic induction in non-uniform thin sheets with an application to the northern Pyrenean induction anomaly, Geophys. J.R. Astron. Soc., **51**: 669-690.

VIDOTTI, R. M., EBINGER, C. J., & FAIRHEAD, J. D. -1995- Flexural rigidity at Parnaíba Basin, Brasil. Proceedings 4th International Congress Braz. Soc. Geophys., **2**:879-879, Rio de Janeiro, Brazil.

VITORELLO, I. & PADILHA, A. L. -1993- Perfis de resistividade AMT: Contribuição ao reconhecimento estrutural da borda sudeste da Bacia do Parnaíba. Revista Brasileira de Geociências, **23**(1): 81-91.

WANG, XI-SHUO, SAMSON, J. C. & GOUGH, D. I. -1987- Wave-number domain analysis of magnetometer array data. J.Geomagn. Geoelectr., **39**: 129-142.

WEAVER, P. -1982- Regional induction in Scotland: an example of three-dimensional numerical modelling using the thin sheet approximaion. Phys. Earth Planet. Inter., **7**: 266-281.

WOODS, D.V. & LILLEY, F. E. M. -1980- Anomalous geomagnetic variations and the concentration of telluric currents in south-west Queensland, Australia. Geophys. J.R.Astron. Soc., **62**: 675-689.

Manuscript submitted December 1, 1998
Revised version accepted April 10, 1999